Site Heterogeneity and Broad Surface-Binding Isotherms in Modern Catalysis: Building Intuition Beyond the Sabatier Principle

James M. Mayer

Department of Chemistry, Yale University, 225 Prospect St., New Haven CT 06520
james.mayer@yale.edu

ABSTRACT: Learning the science of heterogeneous catalysis and electrocatalysis always starts with the simple case of a flat, uniform surface with an ideal adsorbate. It has of course been recognized for a century that real catalysts are more complicated. For the increasingly complex catalysts of the 21st century, this Perspective argues that surface heterogeneity and non-ideal binding isotherms are central features, and their implications need to be incorporated in current thinking. A variety of systems are described herein where catalyst complexity leads to broad, non-Langmuirian surface isotherms for the binding of hydrogen atoms – and this occurs even for ideal, flat Pt(111) surfaces. Modern catalysis employs nanoscale materials whose surfaces have substantial step, edge, corner, impurity, and other defect sites, and they increasingly have both metallic and non-metallic elements M_nX_m, including metal oxides, chalcogenides, pnictides, carbides, doped carbons, etc. The surfaces of such catalysts are often not crystal facets of the bulk phase underneath, and they typically have a variety of potential active sites. Catalytic surfaces *in operando* are often non-stoichiometric, amorphous, dynamic, and impure, and often vary from one part of the surface to another. Understanding of the issues that arise at such nanoscale, multi-element catalysts is just beginning to emerge. Yet these catalysts are widely discussed using Brønsted/Bell-Evans-Polanyi (BEP) relations, volcano plots, Tafel slopes, the Butler-Volmer equation, and other linear free energy relations (LFERs), which all depend on the implicit assumption that the active sites are all "similar" and that surface adsorption is close to ideal. These assumptions underly the ubiquitous intuition based on the Sabatier Principle, that the fastest catalysis will occur when key intermediates have free energies of adsorption that are not too strong nor too weak. Current catalysis research often aims to minimize the complexity of non-ideal isotherms through experimental and computational design (e.g., the use of single crystal surfaces), and these studies are the foundation of the field. *In contrast, this Perspective argues that the heterogeneity of binding sites and binding energies is an inherent strength of these catalysts.* This diversity makes many nanoscale catalysts inherently a high-throughput screen wrapped in a tiny package. Only by making the heterogeneity part of the foundation of catalysis models, sorting the types of active sites and dissecting non-ideal binding isotherms, will modern catalysis learn to harness the inherent diversity of real catalysts. Controlling rather than avoiding diversity is needed to optimize complex modern catalysts and catalytic conditions.

I. Introduction

Further development of heterogenous catalysis and electrocatalysis will require understanding of the binding and reactivity of surface-bound intermediates. While commercially viable catalysts are rarely 'designed,' there are many examples of understanding mechanisms and structure/function relationships being the foundation for remarkable advances. This Perspective modern catalysts becoming more nanoscale and more compositionally complex prompts a re-evaluation of common intuition and approaches.

Understanding the binding and the reactivity of surface intermediates has been a central challenge in catalysis for a hundred years. With the growth of surface science, it became possible to simplify the problem by using clean single crystal metal surfaces as catalysts. This has led to great advances, such as atomic resolution of the individual steps in the catalytic oxidation of CO on a platinum(111) surface.[1, 2] The results from single crystal surface science can, in some situations, be directly connected to catalytic processes.[3]

However, even with well-ordered, effectively defect-free single-crystal metal surfaces, kinetic treatments of surface reactions often make simplifying approximations. Kinetic models frequently—though certainly not always (*cf.* [4,5])—use the assumption that adsorption is *ideal*, that the surface coverage of each adsorbate X (θ_X) follows the Langmuir isotherm.[6] Ideal behavior allows rate and equilibrium expressions to simply use surface coverages, which means that binding energies and reaction barriers are well described by single free energy values (see below).

For traditional catalysts, assuming adsorbate ideality is often sufficient, especially for trends in catalysis by similar surfaces.[6] This has led to a common intuition that non-

ideality does not have a large effect on catalysis. Boudart and Djega-Mariadassou's classic 1984 text *Kinetics of Heterogeneous Catalytic Reactions* derives this conclusion for modestly non-ideal adsorbates whose binding energies vary in a regular way (see below).[7] Somorjai and Li's 700+ page *Introduction to Surface Science and Catalysis* mentions only the Langmuir isotherm and concludes:[8]

> Although the model is physically unrealistic for describing the adsorption of gases on real surfaces, its successes … [are] due to the relative insensitivity of macroscopic adsorption measurements to the atomic details of the adsorption process.[8]

Somorjai and Li's statement is less accurate today because of the complexity of modern catalysts. Modern catalysts are often small nanoparticles or irregular surfaces that have a large proportion of edge, corner, and defect sites. These are more reactive than sites on low-index crystal facets,[9-11] and can make the surface more prone to rearrangement, over time and even within a catalytic cycle.[12-17] Traditional intuition has often been based on noble metal catalysts, while current research is increasingly exploring earth-abundant materials for reasons of cost, scarcity, and sustainability.[18] Many catalysts of current interest are binary and ternary materials, including oxides, chalcogenides, pnictides, carbides, etc.[19-22] The surfaces of such materials often have stoichiometries and structures that differ from the bulk, and their most catalytically active regions can be hydrous and/or amorphous.[23-26] The surfaces of binary materials M_nX_m are often quite reactive, including to air, water, and the sometimes harsh conditions of thermal and electrochemical catalysis. These surfaces are therefore likely to have strongly-bound impurities. All of these properties lead to relatively high levels of surface diversity, in composition, structure, and electronic structure.

Today, the central intuition for heterogeneous catalysis is the century-old Sabatier Principle, that surface intermediates should not bind too strongly or too weakly (Figure 1[27]). However, high surface diversity and non-ideality prompt a reconsideration of this intuition. Figure 1 is almost self-evident for a surface with a single, ideal site. For more complex catalysts that bind substrates at various sites, a single surface bond strength is usually not a sufficient predictor.

The importance of surface diversity and non-ideality was well-known long ago, but this topic often takes a back seat in discussions of modern catalysis. Still, there have always been studies in this area, and the last few years have seen a resurgence (cf., [28-35]). Increasingly powerful analytical tools have shown experimentally that many catalysts are non-ideal and dynamic. A few representative examples could include nanoscale gold catalysts,[36] Fischer-Tropsch catalysts,[37] electrosynthesis,[38] colloidal chalcogenide and pnictide nanoparticles,[39-46] H on metal phosphide catalysts,[47] and the RuO_2 and IrO_2 studies described below. Theoretical and computational studies are re-emphasizing non-ideality and heterogeneity, and the leading studies have much to teach us.[28-31,48-52] It must be emphasized that the statements in this Perspective are not new or unique. The goal here is to raise awareness of surface heterogeneity and non-ideality and their many implications for catalysis.[15,53-57]

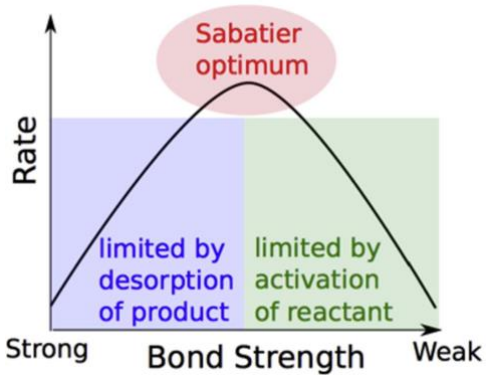

Figure 1. Illustration of the Sabatier Principle.[27] Reprinted from *Journal of Catalysis*, Vol 328, Andrew J. Medford, Aleksandra Vojvodic, Jens S. Hummelshøj, Johannes Voss, Frank Abild-Pedersen, Felix Studt, Thomas Bligaard, Anders Nilsson, Jens K. Nørskov, From the Sabatier principle to a predictive theory of transition-metal heterogeneous catalysis, Page 37, 2015, with permission from Elsevier.

II. Overview of this Perspective

Non-ideal behavior should not be a correction or an afterthought—this is a typical property of catalytic surfaces. Catalysts with multiple kinds of active sites can be valuable, operating under a range of conditions and binding different surface intermediates in various ways. They could potentially be viewed as an all-in-one high-throughput experiment. Single-site catalysts are exciting and attractive for many reasons, but there are challenges in knowing what single structure to aim for. Even for proteins with clearer structure-function relationships and refined computational approaches, a recent deep-learning paper identified 7,648 designs for individual experimental testing.[58] Machine learning approaches are becoming increasingly important in catalysis, using computational and/or experimental datasets.[59-66] In addition to testing many different catalysts, it would be valuable to also examine and harness the inherent diversity in multi-element, nanoscale catalysts.

The focus here is on oxidation/reduction (redox) reactions, and the binding of molecular fragments such as H and OH. In the parlance of inorganic chemistry, these are X-type rather than L- or Z-type ligands.[67-69] The revised intuition advocated here may be less dramatic for the binding of stable molecules such as CO. The examples below largely describe stoichiometric reactions involving surface hydrogen, the X-type adsorbate that has been most studied. Studies of individual reaction steps are a valuable approach to understanding catalytic systems, following the model of homogeneous catalysis.[70] Still, as emphasized by a reviewer, "only true probe of active site chemistry is the kinetic profile of the reaction itself" and the *ex situ* measurements described here need to be considered in that light.

The next few sections establish a common background for the Perspective, introducing various kinds of Linear Free Energy Relationships (LFERs) and surface adsorption isotherms. Connections are made between treatments for surfaces *vs.* homogeneous solutions, and between thermal *vs.* electrochemical reactivity. Systems with non-ideal adsorption are presented in Sections VI, VII, and X. Sections VIII and IX explain how substantial non-ideality

complicates the foundational LFER treatments in catalysis. The Perspective closes with ideas for understanding and harnessing surface diversity and revised LFERs for improved catalysis.

III. Historical View of Heterogeneity and Non-Ideality in Catalysis

Non-ideal surface adsorption—a diversity of surface sites and adsorbate interactions—has long been recognized as an important feature of catalysis and electrocatalysis. Mathematical forms of non-ideal isotherms were introduced in the early 20th century, and they have been extensively used.[71]

A 1958 paper by Parsons derived the shape of volcano plots first assuming ideal Langmuir isotherms, and immediately followed that with a discussion on non-ideality (his Section 4), the start of which is quoted here.[72] Parsons' conclusions are discussed in Section IX.

> 4. Effect of Heterogeneity of Surface or of Interactions Between Adsorbed Hydrogen Atoms: Temkin Model
>
> The feature of the above discussion which is farthest from plausibility is the use of a Langmuir adsorption isotherm since it is well known that the heats of adsorption of hydrogen on metals fall with coverage….[72]

Conway's *Accounts of Chemical Research* article from 1981 emphasizes the multiplicity of sites for an adsorbate A with surface coverage θ_A:[73]

> … results obtained by thermal desorption in gas/solid experiments and especially in electrochemical measurements show that [the equilibrium constant for adsorption] is usually neither independent of θ_A nor a continuous function of θ_A; it often has a series of discrete values over distinguishable small ranges of θ_A as θ_A is changed from 0 to 1. This constitutes the phenomenon of "multiple state" adsorption in monolayers.[73]

For gas-phase hydrogen adsorption on Pt, recent measurements and calculations by García-Diéguez, Hibbitts, and Iglesia found that ΔH_{ads} decreased with increasing surface coverage, by ~30 kJ mol^{-1} (~7 kcal mol^{-1}).[74] Pt nanoparticles (1.6 - 9.1 nm diameter) had ca. 40 kJ mol^{-1} (~10 kcal mol^{-1}) stronger binding than a flat Pt(111) surface. This is:

> because their surfaces expose a larger fraction of low-coordination atoms. The nonuniformity of Pt surfaces, repulsion among co-adsorbates, and high adsorbate mobility starkly contrast with the requirements for Langmuirian descriptions of binding and reactions at surfaces, despite the ubiquitous use and success in practice of the resulting equations in describing adsorption isotherms and reaction rates on surfaces.[74]

Such 'structure sensitivity' is well known for Pt and other catalysts, and has long been recognized to contribute to site heterogeneity in metal nanoparticle surfaces.[4,75-82]

IV. Background 1: Kinetic-Thermodynamic Linear Free Energy Relationships (LFERs), Volcano plots

Surface binding energies have been an important part of catalysis since the Sabatier principle a century ago (Figure 1).[83-85] Quantitatively, the formation and reactions of adsorbates are described by free energies. Kinetic-thermodynamic linear free energy relationships (LFERs) correlate rate parameters, $\ln(k)$ or $\Delta G^{\ddagger}$, with driving force, $\ln(K_{eq})$ or $\Delta G^{\circ}_{reaction}$. In solution chemistry, LFERs have long been a central tool for understanding reactions,[86-92] starting from the Brønsted 'catalysis law' and Evans and Polanyi's generalization to free energies (eqs 1 and 2). Eq 2 is now called a BEP relation, for Brønsted (or Bell)-Evans-Polanyi. BEP relations are widely used in surface reactivity, as illustrated by the 2010 *Chemical Review* "Reactivity Theory of Transition-Metal Surfaces: A Brønsted–Evans–Polanyi Linear Activation Energy–Free-Energy Analysis."[89] The common volcano plots can be viewed as two LFERs that intersect at the Sabatier optimum (Figure 2, see also Section IX).

$$\ln(k) = \alpha \ln(K_{eq}) + \ln(k_0) \quad (1)$$

$$\Delta G^{\ddagger} = \alpha \Delta G^{\circ} + \Delta G_0^{\ddagger} \quad (2)$$

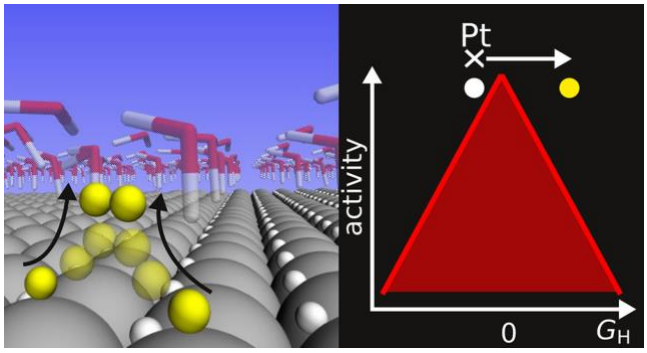

Figure 2. Left: Illustration of the Tafel mechanism for H_2 formation at Pt(111), where two OPD-H atoms (yellow balls) come together to form H_2. The yellow atop OPD-H are distinguished from the inert, silvery UPD-H in hollow sites (see Section VI). Right: Volcano plot correlating catalytic activity with their free energy to bind ½H_2 (G_H). Reprinted (adapted) with permission from *ACS Catal.* **2020**, *10*, 121–128.[93] Copyright 2019 American Chemical Society.

In parallel with LFERs for solution reactions, similar equations were advanced for electrochemical catalysis: the Tafel equation and then the Butler-Volmer equation (eqs 3,4). These relate the current density log(j), a measure of rate, to the overpotential η that describes the driving force. η is the difference between the applied potential and the equilibrium potential under the catalytic conditions (eq 5), and j_0 is the formal current density in each direction at $\eta = 0$. These are very similar to eqs 1 and 2 since $\ln(K_{eq})$, ΔG°, and nE° are conceptually the same in this context (eq 6).

$$\log(j) = \log(j_0) \pm \alpha\eta \frac{2.303F}{RT} \quad (3)$$

$$\log(j) = \log(j_0)\left\{\beta\eta \frac{2.303F}{RT} - (1-\beta)\eta \frac{2.303F}{RT}\right\} \quad (4)$$

$$\eta = E_{\text{applied}} - E_{\text{equilibrium}} \quad (5)$$

$$\Delta G^{\circ} = -RT\ln(K_{eq}) \qquad \Delta G^{\circ} = -nFE^{\circ},\ \Delta G = -nF\eta \quad (6)$$

The central assumption of LFERs, a volcano plots, and the Sabatier Principle is that the reactions being compared are '*similar*.' Often 'similar' is defined intuitively (all metal phosphide surfaces) or in a circular fashion, by taking reactions that follow the same LFER as similar. The question of similarity is central to the application of LFERs and the

Sabatier Principle, and to this Perspective, as discussed in Section V.ii below.

Eqs 1-4 all relate rate to driving force. When the k, $\Delta G^{\ddagger}$, j, K_{eq}, ΔG° and η all refer to a single step, then all the proportionality constants α and β have the same value. Across a series of reactions, α and β report what fraction of the change in driving force appears in the barrier, with values often taken to be ~½.

However, LFERs are often extended beyond their original definition to correlations that involve *overall* rates for a multistep catalytic reactions [log(j), log(k), turnover frequency (TOF)].[94-96] These rates are correlated with thermochemical parameters for one step, or for the entire catalytic cycle (for electrochemical overpotentials). This jump from a single step to a multistep process requires linear *scaling relationships*, which relate the ΔG°_i and $\Delta G^{\ddagger}_i$ of each of the i kinetically significant steps. Scaling with the overall ΔG° or η can also be needed.[97] Such relationships have been established computationally for a variety of systems, predominantly on relatively simple catalytic surfaces.[72,94,98-102] However, such scaling is less likely to hold for multistep catalysis on complex surfaces, that can have different intermediates on different sites. For instance, stepped surfaces have different scaling than flat ones.[90,103] In general, pre-equilibrium steps ln($K_{eq,i}$) scale with 100% of the ΔG°_i for that step (eq 6), while the *barrier* for the rate limiting step scales with only a fraction of the driving force for that step (eq 2).[96]

LFERs are at the center of most semi-quantitative analyses of surface catalysis, and they are a foundation of the long history of volcano plots (e.g., Figure 2 for the HER).[72,91,93-106] Both the rising and falling lines are essentially LFERs that correlate a measure of a catalytic rate (*e.g.*, ln(k) or ln(j)) with a thermochemical descriptor. In Figure 2, the descriptor is the hydrogen binding energy ΔG_H (referenced to H_2).[89] Volcano plots are simplified models[93,99,107] that are widely used as a quantitative implementation of the Sabatier principle. Many sets of catalytic reactions show a volcano relationship and these plots have provided very valuable rationales and predictions.[27,90] Still, the simplifications inherent in these plots are harder to justify for complex multi-element, nanoscale catalysts, as described below.

V. Background 2: Non-ideality and Isotherms

Ideal behavior for an adsorbate X means that its activity a_X parallels its surface coverage θ_X. The definition of an ideal *solution* of X is similar, that the activity of X is given by its concentration [X]. Chemists and chemistry textbooks almost always deal with solutions that are close to ideal. Deviations are notable at high concentrations, for ions in lower-polarity solvents, with strongly-interacting mixed solvents, and in some other situations. These are often the conditions of practical catalysis and electrocatalysis, so catalysis scientists and engineers are in general much more familiar with non-idealities[108-110] (and they can skip this section or object to its simplifications). In this Perspective, a_X is used for *surface activities* and concentrations will be used for solutions (assumed ideal).

i. Site heterogeneity and adsorbate interactions

Adsorption of a species X can be non-ideal for different reasons. Site heterogeneity means that adsorbates can occupy different kinds of sites. These can be different sites on a single-crystal surface, e.g., bridge vs. atop, surface defects such as vacancies or steps, or different elements on the surface (Scheme 1). Non-ideality also results from interactions between adsorbates (blue arrows in Scheme 1).

Scheme 1. Simplified mechanism for X + Y → XY at a single crystal metal surface (top) versus the complexities of X binding to an irregular, impure binary material (bottom) with inter-adsorbate interactions (blue arrows).

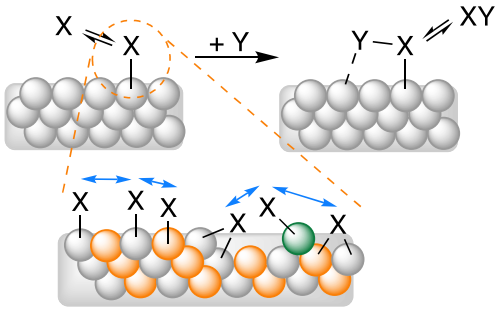

Generally, non-ideality is more common on surfaces than in solution. Gileadi has a particularly clear explanation of this difference:[111]

> [On a pure metal,] there is an average distance of 0.28 nm (2.8Å) between atoms. The equivalent bulk concentration is 78 M, which is evidently much above anything that can be observed experimentally. Thus, we find that the molecules are very crowded on the surface. A relatively low fractional coverage of θ = 0.1 is equivalent to a bulk concentration of about 2.5 M, in which interactions between solute molecules are expected to be the rule, rather than the exception....[111]

He also has a colorful analogy for the presence of multiple surface sites:[111]

> Solid surfaces are rarely homogeneous.... This is much like people entering a movie theater with unmarked seats: the best seats [most negative ΔG_{ads}] are taken first, and the worst remain for late-comers...[111]

One could add that, when possible, most moviegoers prefer to leave open seats between their group and other patrons—a rough analogy with repulsive site-site surface interactions.

The quotes from Gileadi, Parsons, and Conway here and above predate the current movement toward nanoparticle and multi-element catalysts, which makes non-ideality even more important.

ii. Sorting different surface sites

In traditional surface science, analyzing adsorption typically starts with the identification of the different types of surface sites.[112] Often flat crystal and stepped surfaces are investigated separately, as these typically fall on different LFERs.[103,113] Interactions among adsorbates are considered as a correction term, as needed. When distinct sites behave differently, the reaction is said to be 'structure sensitive.'[112] *Sorting into different sites is central to this Perspective, and to any treatment of heterogeneity.*

When comparing different reactions, surface sites, or catalysts, these must be "similar" in order for them to follow

a single LFER, volcano plot, or the Sabatier Principle. The mathematical definition of similarity for this purpose is that eq 2 can be simplified to use $\Delta G°$ as the *only* parameter for the series of reactions (eq 7).

$$\Delta G^{\ddagger} = \alpha \Delta G° + \Delta G_0^{\ddagger} \quad (2) \qquad \Rightarrow \qquad \Delta G^{\ddagger} = f(\Delta G°) \qquad (7)$$

This requires that the α and $\Delta G_0^{\ddagger}$ parameters are constant or vary in a way that is uniquely defined by $\Delta G°$. This simplification has been justified for simple surfaces based on computed scaling relationships. For instance, DFT calculations of energy barriers for A–B bond cleavage reactions (E_{ts}) on flat single crystal metal surfaces scale very well for different metals and different bonds, with eq 7 becoming $E_{ts} = 0.84E_{diss}$(A–B) + 1.92.[90] Still, the scaling is different for stepped surfaces.[90,103]

The simplest and most common sorting, first proposed by Boudart, is to use a find Most Abundant Reactive Intermediate (MARI) and perhaps a Most Abundant Surface Intermediate (MASI), when these can be identified and quantified.[114,115] This is often a sufficient first approximation. When comparing different catalysts, it adds the assumptions of common MARI and MASI species and coverages.

An additional complication is that eqs 2 and 7 implicitly assume Langmuir isotherms (unless all the parameters become functions of θ). Non-ideal adsorption adds additional features that must follow requirements for similarity such as scaling relationships (see below).

It is the hypothesis of this Perspective that the simplification in eq 7 cannot be done for complex, nanoscale surfaces composed of multiple elements, and that scaling relationships will not hold. The α and $\Delta G_0^{\ddagger}$ parameters depend on many things beyond $\Delta G°$, such as whether the reactive H is bound to one element or another, or in an atop vs. a 3-fold vs. a step site. It is my hope that this hypothesis will be tested by experiments and computations that include the full complexity of nanoscale M_nX_m and single entity[116] catalysts under operating conditions.

The challenge is that there is usually little or no understanding of how to do this sorting for complex surfaces. The number and nature of the various sites, their energetics, and their reactivity are challenging to explore. For instance, in the Fischer-Tropsch process, the stoichiometry, surfaces, and binding sites for H, CO, and $C_xH_yO_z$ intermediates on the nanoscale iron-carbide particles are essentially unknown. The use of complex surfaces with various sites brings the sorting problem to the fore.

Therefore, it is valuable to measure a binding isotherm for a surface in its entirety, without any sorting. The isotherm will likely cover multiple kinds of sites and could provide insight into the sorting process, as discussed below.

A brief foray into metal oxide surfaces illustrates the sorting challenges, and it sets the stage for the case studies below. Redox reactions of oxides in contact with protic media generally occur by proton-coupled electron transfer (PCET), the transfer of $H^+ + e^-$ or, equivalently, a hydrogen atom ($H^•$).[117,118] Scheme 2 sketches a few possible pathways for oxidation of a protonated or hydrated surface. The proton can be transferred from an oxygen that part of the lattice or from a surface hydroxide or water molecule. The oxide or hydroxide formed upon H^+ loss could become part of the lattice. More generally, the less crystalline the surface, the more hydrated, porous, and amorphous, the less meaningful is any distinction between lattice O and adatom sites, and the more muddied are the definitions of surface sites and surface coverages.

Scheme 2: H-atom loss from a hydrated metal oxide surface could occur from a lattice oxygen, a surface hydroxide, or a weakly bound water molecule. The green boxes indicate the oxide lattice, but this distinction is likely less clear in practice.

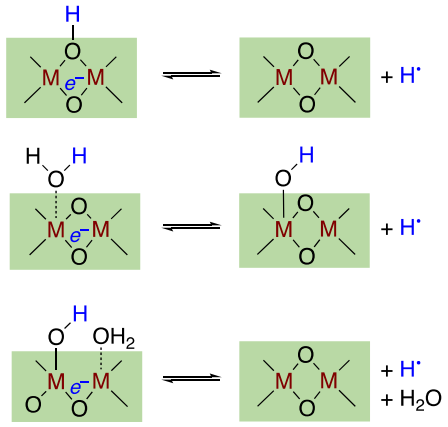

The challenges in sorting blur the traditional distinction between surface heterogeneity and adsorbate-adsorbate interactions. These effects are also often comingled in experimental measurements. Therefore, adsorption will be described here just as 'non-ideal,' in most cases without specifying an origin.

iii. Characteristics of ideal and non-ideal adsorption

Ideal adsorption is characterized by a single free energy of adsorption, $\Delta G°_{ads}$. We primarily use here $\theta = ½$ as the standard state for $\Delta G°_{ads}$. This allows direct analogies with the typical solution standard state where all dissolved species have equal concentrations (1 M for ideal solutions). The analogous situation on a surface is when half the surface sites are occupied by the adsorbate, $\theta = (1 - \theta) = ½$.

A common alternative surface standard state uses the properties of the adsorbate at low coverage, $\theta \to 0$, extrapolated to $\theta = 1$ (though see [119-123]). The $\theta \to 0$ extrapolation avoids interactions between adsorbates but is less intuitive.

When adsorption is non-ideal, the *apparent* free energy of adsorption is a function of coverage: $\overline{\Delta G}°_{ads}(\theta)$, and the activity a_X need not be proportional to θ_X. Non-ideality makes kinetic and equilibrium expressions complex, so it is helpful to use a qualitative metric such as the width of the free energy isotherm described by $\overline{\Delta G}°_{ads}(\theta)$. This width is roughly equivalent to the range of surface–X bond dissociation free energies (BDFEs) and to the width of an anodic or cathodic peak in a cyclic voltammogram (CV).

Moderately wide isotherms have only a modest effect on kinetic parameters. Adsorbates with $\overline{\Delta G}°_{ads}$ 2.7 kcal mol^{-1} (120 meV) weaker than the $\theta = ½$ standard state $\Delta G°_{ads}$ should undergo reactions roughly ten times faster than

adsorbates at $\theta = ½$ (at 298 K using eqs 1,2 with $\alpha = ½$). However, this increase in k is often offset by the lower population of more weakly bound sites. This balance is the origin of the traditional intuition that moderate non-ideality of a single active site is not typically an important factor in catalytic reactions (though see [34]).

iv. Ideal behavior: the Langmuir isotherm

Ideal adsorption of X is described mathematically by the Langmuir isotherm, shown in one form in eq 8. For a molecular adsorbate like CO, the activity is taken as its partial pressure or its solution concentration. When the X is an unstable fragment, such as a hydrogen atom, a_X is often referenced indirectly, for instance H• to H_2 gas.

$$\frac{\theta}{1-\theta} = K_{eq}[X] = \left(e^{-\Delta G^\circ/RT}\right)[X] \quad (8)$$

$$A + X \rightleftharpoons AX \qquad \frac{[AX]}{[A]} = K_{eq}[X] \quad (9)$$

$$Ox + e^- \rightleftharpoons Red \qquad E = E^\circ - \frac{RT}{nF}\ln\left(\frac{[Red]}{[Ox]}\right) \quad (10)$$

$$\overline{\Delta G}_{ads}(\theta) = \Delta G^\circ_{ads} + \frac{RT}{F} ln\left(\frac{\theta}{(1-\theta)}\right) \quad (11)$$

The Langmuir isotherm for X binding to a surface is mathematically identical to the equilibrium expression for X binding to a solution species (eq 9), and to the Nernst equation (eq 10). The $\theta/(1\text{-}\theta)$ term is analogous to the ratio of bound-to-unbound ([AX]/[A]) or reduced-to-oxidized ([Red]/[Ox]). The Langmuir isotherm can also be written in parallel to the Nernst equation, as a coverage-dependent free energy $\overline{\Delta G}_{ads}(\theta)$ (eq 11). Just as the effective acidity of a buffer varies from the K_a when [Acid] ≠ [Base], and the potential varies from E° when [Red] ≠ [Ox], $\overline{\Delta G}_{ads}(\theta)$ has a Gaussian distribution around ΔG°_{ads}. All of these have a full-width at half-max (FWHM) of 90 mV (2 kcal mol^{-1}, or a 30-fold change in concentration).

v. Non-ideal behavior: Frumkin and Temkin isotherms

Adsorption is said to be non-ideal when the coverage-dependent free energy $\overline{\Delta G}_{ads}(\theta)$ does not follow a Langmuir isotherm. A common way to treat this is to simply add a term that is linear with θ. Eq 12 shows one version of the Frumkin isotherm as a Langmuir isotherm with an added $C(\theta - 0.5)$ term. The Temkin isotherm is simpler, omitting the $\theta/(1-\theta)$ term. These are two of the many isotherms, which can each expressed in different ways and used for various purposes.[71, 86,124] The parameter C of the added term has units of free energy, often given as unitless $f = C/RT$. Since the $C(\theta - 0.5)$ term is zero at the $\theta = 0.5$ standard state, all of these isotherms have the same standard state ΔG°_{ads}, but the Frumkin and Temkin isotherms are wider ($C > 0$) or narrower ($C < 0$) than the ideal Langmuir.

$$\overline{\Delta G}_{ads}(\theta) = \Delta G^\circ_{ads} + \frac{RT}{nF} ln\left(\frac{\theta}{(1-\theta)}\right) + C(\theta - 0.5) \quad (12)$$
(Frumkin)

$$\overline{\Delta G}_{ads}(\theta) = \Delta G^\circ_{ads} + C(\theta - 0.5) \quad \text{(Temkin)} \quad (13)$$

The Frumkin and Temkin isotherms were originally introduced to model inter-adsorbate interactions, though they are also useful when the origin of the non-ideality is not known. When the C term is small (and at low θ with a $\theta = 0$ standard state), eq 12 reduces to the Langmuir isotherm (eq 11). Alternatively, when C is large, or when θ is close to ½ and $\theta/(1-\theta)$ is close to 1, then the isotherm is dominated by the new linear term. Then the Frumkin and Temkin isotherms are the same (eq 12 => eq 13), and the dependence of the coverage on free energy is *linear*. This contrasts with ideal behavior, where concentrations, rate constants, and equilibrium constants for solutes and adsorbates vary *exponentially* with energies, not linearly.

The isotherms plotted in Figure 3[86] show the difference between the Langmuir isotherm ($f = 0$) versus the Frumkin isotherms with linear sections that vary with f [$C = f(0.59$ kcal mol^{-1}) at 298 K]. The horizontal axis is the driving force, using the $\theta \rightarrow 0$ standard state, plotted as the applied electrochemical potential minus E° (bottom axis) and as $\overline{\Delta G}_{ads}(\theta) - \Delta G^\circ_{ads}$ (top axis). The equivalent plot using the $\theta = ½$ standard state has the same curves, just shifted so that the isotherms all intersect at $\theta = 0.5$, where $(E - E^\circ) = (\overline{\Delta G}_{ads}(\theta) - \Delta G^\circ_{ads}) = 0$.

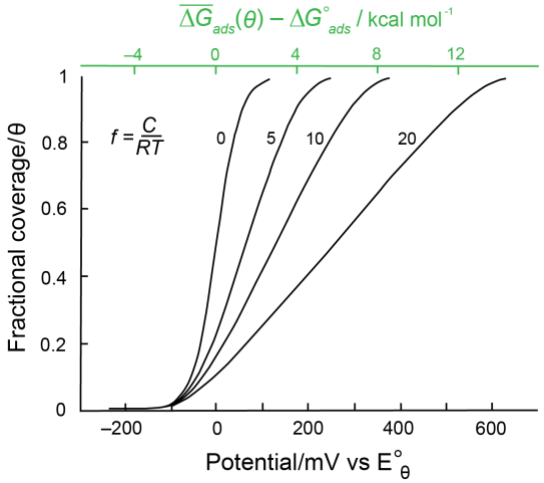

Figure 3. The dependence of θ on applied potential for different values of the unitless parameter $f = r/RT$. $f = 0$ corresponds to the Langmuir isotherm. The potentials are vs. the standard potential, using the $\theta \rightarrow 0$ standard state [and X at standard state, eq 8]. $e(E_{applied} - E^\circ_\theta)$ and $\overline{\Delta G}_{ads}(\theta) = \Delta G^\circ_{ads}$ are the relative free energy of adsorption vs. that standard state. The equivalent plot with the $\theta = 0.5$ standard state used in this Perspective has the same curves, just shifted so that they all intersect at $\theta = 0.5$ (zero driving force). Reproduced and adapted from *Electrode Kinetics for Chemists, Chemical Engineers and Materials Scientists:* Gileadi, E. 1996, figure 2I, p. 268.[86] Reproduced with permission of John Wiley and Sons and Copyright Clearance Center.

One implication of the linear dependence of θ on energy for the Frumkin isotherm is that the population of adsorbates in each energy range $(d\theta/d\Delta G)$ is roughly constant. In this case, the faster rates for more weakly-bound adsorbates are *not* offset by a lower population. This balance was described above as an origin of the intuition that broad isotherms do not strongly affect rate constants. A flat region of a $d\theta/d\Delta G$ plot indicates a Frumkin isotherm, as in the roughly rectangular section for UPD-hydrogen on Pt(111) at the left of Figure 4 in the next section. The challenges of developing LFERs for non-ideal adsorbates are raised below (Section VIII).

As a final general comment, LFERs give barriers and rate constants but catalysis depends on *rates* rather than rate constants. This is emphasized in the degree of rate control analysis,[54,99-102,114,115] and is why Tafel slopes for multistep reactions depend on the sequence of elementary steps, pre-

equilibria, barriers, and surface coverages.[72,94,98-101] One example is the oxidation of ammonia over noble metal surfaces, for which the selectivity between N_2, NO, and N_2O is calculated to be due to relative surface coverages on Pt and Pd rather than differences in barriers (as for Rh).[102]

A recent *Chemical Review* provides a detailed mathematical analysis of complex reversible reactions, including non-idealities, concluding with:[54]

> There is, therefore, a pressing need for the development of analytical diagnostics which enable identification of geometric and/or electronic effects outside of goodness-of-fit to conventional metrics such as reaction order or activation energy. Is there, for example, a kinetic or thermodynamic "signature" of site-ensemble requirements or lateral adsorbate interactions which can be elicited from steady-state or transient rate measurements either near or far from equilibrium?[54]

VI. Hydrogen on Pt(111)

This Perspective emphasizes isotherms for hydrogen adsorption (*H) because H transfers are involved in many kinds of catalysis, and because its isotherms are the most studied.[125-138] While H might be thought of as a simple adatom, its isotherms are often not simple.

The cyclic voltammogram (CV) for a Pt(111) surface in aqueous 0.1 M $HClO_4$ is remarkably complex (Figure 4), given the simplicity of the system. The single-crystal surface is flat with identical surface Pt atoms, and the only relevant solution species are H_2O and H_3O^+ (ClO_4^- is chemically inert). The CV is truncated just above the H_2 thermodynamic potential (0 V vs. the reversible hydrogen electrode, RHE, eq 14) because Pt is an exceptional HER catalyst and the cathodic current becomes large approaching 0 V.

$$H^+ + e^- \rightleftharpoons \tfrac{1}{2}H_2 \qquad (14)$$

definition of the HER and the RHE

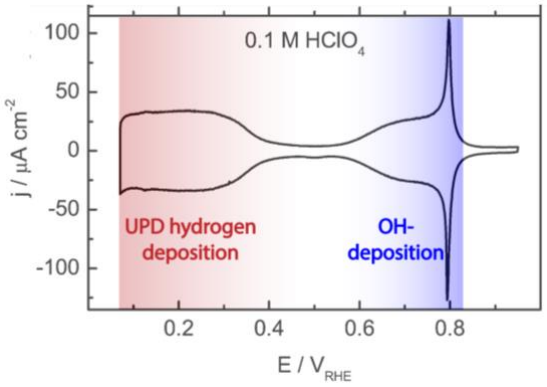

Figure 4. Cyclic voltammogram of Pt(111) in 0.1 M $HClO_4$, with labels for the UPD-H and OH adsorption regions added[139]. Adapted from García, G.; Koper, M. T. M. *Phys. Chem. Chem. Phys.* **2008**, *10*, 3802[139] with permission from the Royal Society of Chemistry.

The mirror relationship between the anodic and cathodic currents shows that the CV reports on thermodynamic properties. When potentials are referenced to RHE, then $FE°$ is the same as the traditional surface-science measure of H affinity, the free energy for addition of $\tfrac{1}{2}H_2$ (ΔG_H, eq 15). $E°$ vs. RHE, ΔG_H, and the surface–H bond dissociation free energies (BDFEs, eq 16) are all conceptually the same.[118]

$$-FE_{RHE}(X + H^+ + e^- \rightarrow XH) = \Delta G°(X + \tfrac{1}{2}H_2 \rightarrow XH) = \Delta G_H \qquad (15)$$

$$\begin{aligned} BDFE(X–H) &= \Delta G° \text{ for: } X–H \rightarrow X + H \\ &= 52.8 — \Delta G_H \text{ (all in kcal mol}^{-1}\text{)} \\ &= 2.29 — \Delta G_H \text{ (all in eV)} \end{aligned} \qquad (16)$$

The feature at the left of the CV in Figure 4 is due to the underpotential deposition of hydrogen (UPD-H), so named because H is added to the Pt surface *under* the potential needed to form H_2 ($V_{RHE} > 0$). The electrochemical process is called the Volmer reaction, and it forms the same UPD-H as from Pt(111) and H_2 gas in the same aqueous media (Scheme 3). The CV measures the current ($d[\#e^-]/dt$), so the shape of the CV wave is the derivative of the coverage vs. applied potential (Figure 3 vs. Figure 4). The UPD-H feature is at least 300 mV wide, much wider than the Langmuir isotherm's Gaussian 90 mV. The flat top of this feature implicates a Frumkin isotherm with a repulsive interaction between surface H, with $C \cong +250$ mV (+6 kcal mol^{-1}).

Scheme 3: Formation of surface H by proton reduction (the Volmer reaction, left and center), and by addition of H_2 (right).

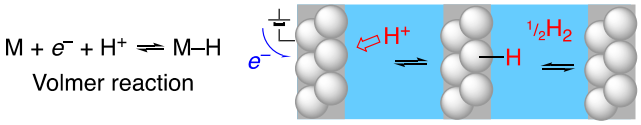

At higher potentials, the complex CV shape for Pt(111) is due to the deposition of hydroxide. The broad feature starting at ~0.6 V is the initial accumulation of surface OH ($C > 0$), then the sharp feature (~0.78 V) indicates cooperative adsorption to form an ordered monolayer ($C < 0$). Catalysis on Pt(111) at high potentials is strongly influenced by this isotherm.[79,140-142] It should also be noted that the isotherms are different on different Pt crystal faces.

There is general consensus that Pt(111) has a second, more important kind of adsorbed H: *overpotential* deposited H (OPD-H).[129-131,143-146] OPD-H is very active in catalysis, forming H_2 and hydrogenating substrates, while UPD-H is quite unreactive. The isotherm for OPD-H is more challenging to examine because of the rapid H_2 formation, but an atop site is indicated by the ν(PtH) IR adsorption at 2050 ± 50 cm^{-1} (depending on the conditions) and its appropriate shifting in D_2O.[129-131,143-147] UPD-H, however, lies in a three-fold hollow site. Computational studies in general support this picture.[93,148]

The message of H on Pt(111) is that there are two kinds of H that are very different in structure and reactivity. Kinetic treatments of H-transfer reactions on Pt(111) have only considered the OPD-H because of the unreactive nature of UPD-H. The *complete* isotherm for H on Pt(111), however, would include both UPD-H and OPD-H. This illustrates the importance of sorting into distinct sites (Section V.ii above). However, such sorting is not yet possible for the more complex catalysts being currently developed.

Pt(111) is one of the simplest, most ordered, and most studied catalytic surfaces. Even on this surface, the isotherm is not simple. *Adsorbates and intermediates on most catalytic surfaces have complex isotherms that impact catalysis.*

VII. Diversity of Hydrogen on Metal Oxides

Metal oxides can be active catalysts, co-catalysts, and catalyst supports. Examples include IrO_2 and others for the OER[25,149-151] and cerium oxide in automotive 'three-way catalysts.'[152,153] Oxide surfaces have received great attention, from single crystals in ultra-high vacuum (UHV) to minerals in natural waters,[154-156] including the thermochemistry of bulk oxides and hydroxides.[157,158] Still, the surface binding or loss of molecular fragments such as H or O is only beginning to be documented.[155]

Addition of an H atom is equivalent to addition of a proton and an electron ($H^{\bullet} = e^{-} + H^{+}$) or ½ H_2. H can be added in a chemical or electrochemical PCET reaction, as in Schemes 2 and 3 above.[117,118] Addition of H atoms to a metal oxide generally forms a surface hydroxide and adds an electron to metal-based orbitals, so H is an *n*-dopant.[159] The electron can be added to an ion with a localized valence (Ce^{3+} in CeO_2, Figure 5A), to an *n*-type multi-metallic trap state (TiO_2), or to a metallic band structure (IrO_2). Protons are ubiquitous on oxide surfaces exposed to air or water, as hydroxides or bound H_2O.[160]

i. H on colloidal ceria nanocrystals

Colloidal cerium oxide nanoparticles (NPs) are a relatively simple system that has been found to be a highly non-ideal. Suspended in THF, with oleate capping ligands, these ~1.8 nm NPs react reversibly with soluble H-atom transfer (HAT) reagents, such as 2,6-dimethyl-hydroquinone (Figure 5B).[161-163] The stoichiometry of this reaction was experimentally established, that it only exchanges H atoms. Therefore, at equilibrium, the affinity of the NPs for H is the same as that of the reagent: the O–H surface BDFE of the NPs is equal to the average O–H BDFE of the reagent. Measuring the equilibrium stoichiometry with reagents of different BDFEs mapped out the isotherm for H-binding to the ceria NPs (Figure 5C).[162]

The measured CeO–H BDFEs span 13 kcal mol^{-1} (0.56 eV) with changes in the average redox state of the surface of the nanoceria colloid (Figure 5A,C).[162] At higher $\%Ce^{3+}$, adding $H^{\bullet}$ is more difficult implying weaker O–H BDFEs. The BDFE variation corresponds to a change of *10^9 in equilibrium constant* for HAT. The wide range is likely due to increasing lattice strain as more Ce^{4+} is converted to larger Ce^{3+} ions. The strain makes it more difficult to accommodate more Ce^{3+} ions, and therefore weakens the O–H bonds formed. The mostly linear shape of Fig. 5C indicates that these data can be well fit to a Frumkin isotherm.

A subsequent study examined the kinetics of H-atom transfer from $CeO_{2-x}H_y$ to the hydrazyl radical DPPH as a function of θ_H.[163] By using only a small amount of DPPH, the θ_H, CeO-H BDFE, and $\Delta G°_{HAT}$ did not change significantly over the reaction. Rate constants for reactions initially poised at different θ_H gave a LFER connecting $\ln(k_{HAT})$ with $\ln(K_{eq})$, the latter from the $\Delta G°_{HAT}$ of each reaction. The linear relationship showed that all of the CeO–H species belonged to the same type of surface H, though the BDFE was changing substantially. Surprisingly, the Brønsted α for these reactions was only 0.2, much less that the often-assumed 0.5.

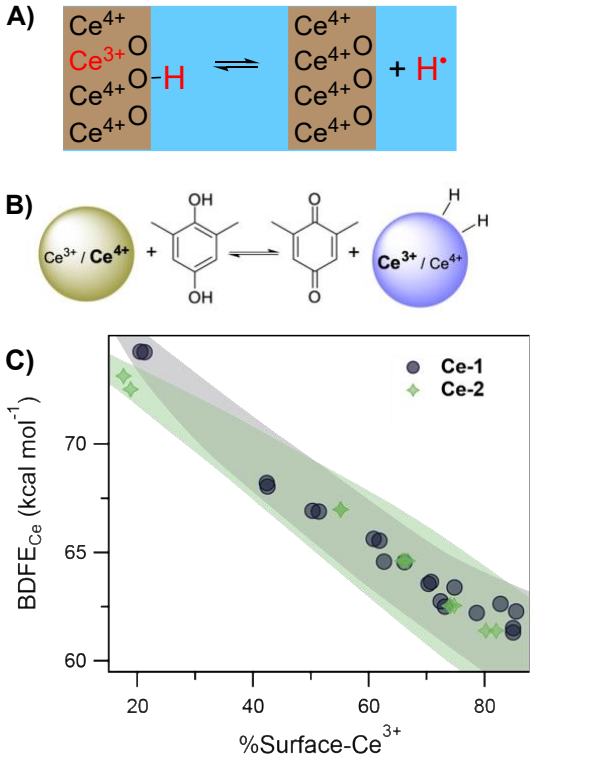

Figure 5. **A)** Schematic of H-atom addition and removal from a cerium oxide (ceria) surface. The free energy of the forward reaction is the surface O–H BDFE. **B)** At equilibrium between colloidal $CeO_{2-x}H_y$ NPs and a hydroquinone/quinone couple, the CeO–H BDFE ($BDFE_{Ce}$) is that same as the average BDFE in the H_2Q. **C)** Plot of $BDFE_{Ce}$ vs. % surface Ce^{3+} of two batches of $CeO_{2-x}H_y$ NPs. The shaded regions show the estimated uncertainties. **B** and **C** Reprinted (adapted) with permission from *J. Am. Chem. Soc.* **2021**, *143*, 2896.[162] Copyright 2021 American Chemical Society.

ii. H on nickel oxide

NiO has been widely studied as an earth abundant p-type semiconducting oxides, and–with some iron–a good water oxidation electrocatalysts. In this Perspective, electrochemical studies of NiO thin films are introduced as a compliment to the thermal reactions of ceria NPs in the last section. NiO has long been known to typically show Ni^{3+}/Ni^{2+} and Ni^{4+}/Ni^{3+} PCET redox couples (*e.g.*, eq 17).[164,165] Eq 17 also shows the $Ni(OH)_2/NiO + H_2O$ equilibrium to indicate the complexity of hydrous metal oxides.

$$Ni^{3+}(O)(OH) \xrightarrow[\text{or } + H^{\bullet}]{+ H^{+} + e^{-}} Ni^{2+}(OH)_2 \rightleftharpoons NiO + H_2O \quad (17)$$

The NiO–H isotherm was measured by spectroelectrochemistry, at each of the potentials shown by dotted lines over the CV in 65A.[165] For the $NiOOH/Ni(OH)_2$ couple, the $\%Ni^{2+}$ was taken as equal to the θ_H, following eq 17. The data followed a Frumkin isotherm (solid line in Figure 6B) rather than ideal behavior (dashed line). The Frumkin *C* parameter was 6 kcal mol^{-1} (0.25 eV).[165]

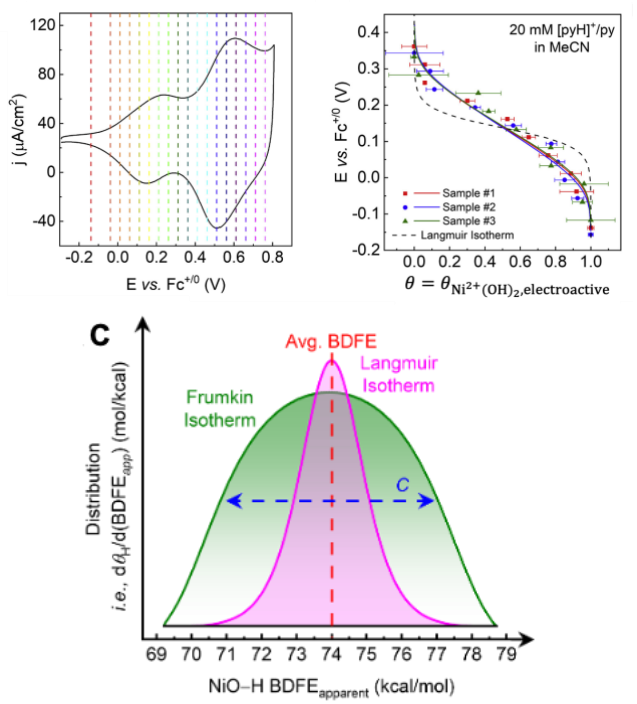

Figure 6. A) CV of a NiO thin film in pyH^+/py buffered MeCN. **B)** $\theta_H = \theta_{Ni^{2+}}$ at each of the potentials shown in A) by the vertical dashed lines. The solid black line is the fit of three datasets to a single Frumkin isotherm; the dashed line is the best Langmuir isotherm fit. **C)** Representation of the NiO isotherm as a range of BDFEs (green) that is much wider than the ideal Langmuir isotherm. Permission *requested*. [Reprinted with permission from *Chem.* **2022**, *8*, 3324-3345. Copyright 2022 Cell Press.]

Similar measurements were done in aqueous solutions and 'dry' organic solvents (MeCN and DMF), and with a wide range of different buffers, over 10^{16} in proton activity. Remarkably, *all of the isotherms were the same* when referenced to RHE. The center of each isotherm, the average NiO–H BDFE, was 74 ± 2 kcal mol^{-1} under all conditions, and the Frumkin *C* parameters were all the same. This was not expected for electrochemical measurements under quite different conditions. However, such solvent and medium independence is typical of molecular hydrogen atom transfer reactions.[118] Thus even this electrochemical reaction has the character of H• transfer (eq 17 under the arrow).

iii. H on IrO_2 and RuO_2

IrO_2 and RuO_2 are among the most active metal oxides for redox catalysis such as the OER, with the most active forms believed to be porous and in part amorphous.[24,166-175,] RuO_2 is used commercially in the dimensionally stable anodes (DSA) to produce Cl_2 as part of the large-volume chlor-alkali process.[176-178] These oxides have been studied in great detail and *in operando* experiments are generating many new insights.[25,26,170,173,182] Two recent sets of studies have emphasized isotherms and are interesting to compare. Suntivich *et al.* have examined highly ordered epitaxial thin films of IrO_2(110) and RuO_2(110) on TiO_2,[171-172] while the groups of Stephens, Durrant, and Rao (SDR) have collaborated to examine hydrous, amorphous iridium oxide films electrodeposited on FTO.[173]

Both studies reported two reversible redox features in electrochemical experiments (SDR observed a third). Most of the metal ions in the porous film were electroactive, in contrast to only the undercoordinated sites (ucs) at the surface of the crystalline sample. Suntivich *et al.* described the electrochemical process as the binding energies for *OH and *O to Ir ucs.[171-172] However, the PCET description[117,118] used by SDR seems more reasonable to us, as the DFT calculated structures of IrO_2(110)(*OH) and IrO_2(110)(*O) differ by an H atom (Figure 7B and C).[171] One redox couple was assigned as PCET from a water perhaps weakly bound to an Ir ucs (eq 19; cf. Scheme 2 above).

$$IrO_2(*OH) \rightleftharpoons IrO_2(*O) + e^- + H^+ \quad (\equiv H^\bullet) \qquad (18)$$

$$IrO_2(H_2O) \rightleftharpoons IrO_2(*OH) + e^- + H^+ \quad (\equiv H^\bullet) \qquad (19)$$

The isotherms reported in these studies were non-ideal, and they needed to be fit with Frumkin rather than Langmuir isotherms. The Frumkin *C* parameters for the $MO_2^{4+/5+}$ couples were similar (3-7 kcal mol^{-1}), both for highly ordered crystalline films and for the disordered, porous, amorphous films. This rough independence of the non-ideality on the form of the catalyst is surprising. It suggests that the apparent repulsion between the adsorbates ($C > 0$) is not due to a direct through space interaction, or due to surface inhomogeneity. The observed similarity supports the interpretation by both teams that the apparent repulsion is mediated through the aqueous double-layer.

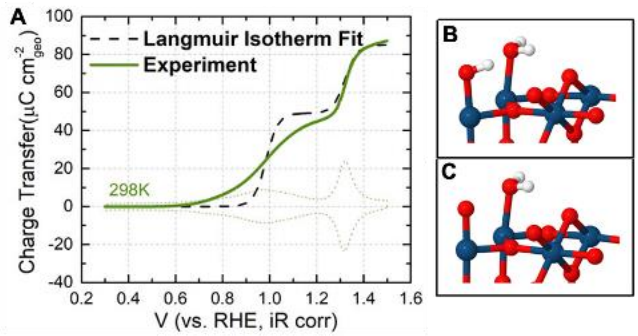

Figure 7. A) Plot of charge transferred (Q) vs. potential, which is the isotherm, for an RuO_2(110) thin film in 0.1 M KOH. The fainted dotted trace is the CV (dQ/dV). The dashed best-fit line shows that using two Langmuir isotherms does not follow the data. **B)** and **C)** are portions of the DFT-computed structures for IrO_2(100)(*OH) and IrO_2(100)(*O), respectively, with the OH and O at the upper left (Ir in blue-grey). Part **A** reprinted with permission *requested* from Hu, B.; Kuo, D.-Y.; Paik, H.; Schlom, D. G.; Suntivich, J. *J. Chem. Phys.* 152, 094704 (2020).[32] Copyright 2020 AIP Publishing. Parts **B** and **C** reprinted with permission *Journal of the American Chemical Society* **2017**, *139*, 3473-3479.[171]
Copyright 2021 American Chemical Society

The redox couples measured in these and other studies of IrO_2 shift with pH, usually more than the predicted Nernstian shift of 59 mV per pH expected for $1H^+/1e^-$ stoichiometries (19 and 20, *E* vs. SHE). Both teams interpreted this shift as being due to Ir–O bonds became stronger at higher pH, while still retaining the $1H^+/1e^-$ chemical processes. However, the same >59 mV per pH "super-Nernstian" shift for many hydrated oxides has been interpreted differently in the pseudo-capacitor literature, including for RuO_2.[183,184] In that field, super-Nernstian behavior indicates a stoichiometry with more than one H^+ per e^-. In one TiO_2 system, there is evidence for a class of trap states with a $2H^+$ per $1e^-$

stoichiometry.[185] These issues illustrate the complexity of oxide surfaces, as discussed in Section V.ii above. Most important, this discussion emphasizes *the critical role of surface stoichiometry*, even if that is difficult to determine. Understanding the OER by IrO_2 will require measuring H^+:e^- and H:O:Ir surface stoichiometries through each of the intermediates.

iv. H on TiO_2

TiO_2 is one of the most studied oxides, in its many forms.[186-189] Here only one computational study is described, the perhaps extreme case of surface TiO–H BDFEs.[190] One set of TiO–H was formed *in silico* by adding H• to the TiO_2 surface, yielding a *OH coupled to e^- in a Ti d trap state (TiO_2•e^-,H^+, roughly $Ti^{3+}OH$). This set was compared with surface OH groups formed by non-redox hydration of the TiO_2 surface: $(Ti^{4+})_2O^{2-} + H_2O \rightarrow 2(Ti^{4+}OH^-)$ (Figure 8A and B).

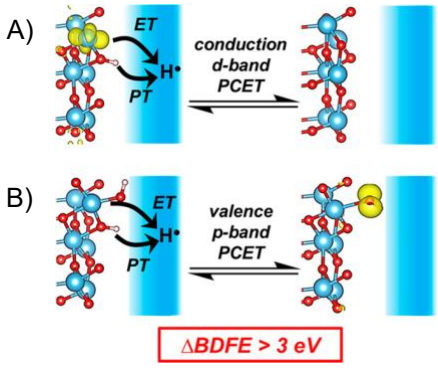

Figure 8. A) PCET from a Ti d-band state, formally $[TiO_2]^-[H]^+ \rightarrow [TiO_2]^0 + (H^+ + e^-)$, and PCET from **B)** an O p-band state, $[TiO_2]^0[OH]^-[H]^+ \rightarrow [TiO_2]^0[O^•] + (H^+ + e^-)$. The converged geometries for each structure have a yellow isosurface representing the charge density associated with the Ti^{3+} polaron (top) or valence band hole (bottom).[190] Reprinted (adapted) with permission from *J. Phys. Chem. Lett.* **2021**, *12*, 40, 9761–9767. Copyright 2021 American Chemical Society.

The computed BDFE for the Ti^{3+}O–H bonds in TiO_2•e^-,H^+ was ca. 40 kcal mol^{-1}. The Ti^{4+}O–H bond, however, was *dramatically* stronger, ~120 kcal mol. (The examples within each of the sets were found to be similar.) The difference of ~80 kcal mol^{-1} (~3.5 eV) is remarkable, especially for O–H bonds that are very similar in structure, bond length, and stretching frequency. The Ti^{3+}O–H bonds are very weak (thermodynamically uphill of H_2) while the Ti^{4+}O–H BDFE is close to that in H_2O. Previous experimental data for TiO_2 films, TiO_2 colloids, and molecular $Ti^{3+}OH$ compounds, also have low BDFE.[188,191]

The primary difference between these two O-H bonds is the source of the electron being removed to make H•. For "Ti^{3+}O–H," the e^- comes from a high-energy trap state near the conduction band. For Ti^{4+}O–H, however, the e^- is removed from a low-energy O lone pair near the valence band to leave an oxyl radical.[190]

Thus, typical *n*-type TiO_2 surfaces in contact with water are covered with identical-*looking* hydroxyl groups, some of which have very strong O–H bonds (like water) and others have very weak O–H bonds that are better H-atom donors than H_2. The different classes of O–H groups are distinguished by the presence or absence of a high-energy trap-state electron that can be transferred with the proton. From a thermochemical perspective, the e^- and H^+ could be quite distant from each other, as long as their transfer doesn't lead to an unfavorable buildup of charge. Molecular PCET reactions have been observed when the proton and electron were more than 1 nm apart in the reactants or products.[192] The full isotherm for H on TiO_2 thus has structurally similar components highly separated in energy.

VIII. LFERs with broad isotherms

For the reasons developed above, LFERs are much more complicated for elementary reaction steps involving adsorbates with non-ideal binding isotherms, vs. the ideal cases in Section IV. Therefore, most treatments of LFERs and volcano plots assume ideality (though certainly not all treatments, *e.g.*,[28,108,193-196]). In the context of the current Perspective, there are a number of issues to highlight.

First, LFERs require free energies, and determining $\Delta G°$ starts with defining a standard state. The $\theta = ½$ standard state at first glance seems closer to the Sabatier principle and easier to apply. However, when the variety of sites and their activities, densities and populations are not known, "$\theta = ½$" is challenging.

Consider OPD-H and UPD-H on the ideal Pt(111) surface (Section VI above). In this case, $\theta_H = ½$ could refer to *i*) half of the UPD-H sites being occupied, *ii*) half of the OPD sites occupied, or the *iii*) half of all the sites occupied (most of the UPD and few of the OPD). Choices *i*) and *iii*) are unreasonable given the inertness of UPD-H and the high HER activity of Pt(111), and ii) is ill-defined due to our limited understanding of OPD-H. The $\theta = 0$ standard state would not include any of the OPD active sites on Pt(111). If very little OPD-H is formed at RHE ($\Delta G°H = 0$), this free energy would unlikely be the point of highest activity—as concluded by Peterson *et al.* (Figure 2 above).[93]

Broad overall isotherms also can complicate the "sorting challenge" (Section V.ii), that is, knowing which materials and reactions are similar enough to be treated with a single LFER or volcano plot. In some cases different sites on the same surface need to be treated with different BEP correlations, such as step sites vs. terraces on a metal surface.[90,91,197] As one example of a more complex process, the lowest energy path for H_2 loss from hydrogenated Mo_2N was computed to be the heterolytic combination of a hydridic MoH with a protic NH.[198] In this case, using *H for a generic surface hydrogen is not appropriate—there are (at least) two kinds of *H with quite different properties. Such issues are expected to be common for multi-element, nanoscale catalysts that have a range of sites and mechanisms.

The recasting of LFERs for broad isotherms has been the subject of many studies over many years, including [4,72,124,193-196,199-205]. This has been done algebraically, such as with the simplified Frumkin formula (eq 12), and with numerical treatments using experimental isotherms such as for OH on Pt(111) (Figure 4). However, neither is a simple task. Kinetic and thermodynamic treatments of non-ideal situations are complex because rate 'constants' and apparent free energies vary with coverage.

The mathematical treatments often require the Brønsted law to connect energies to rate constants (eq 1), and typically assume $\alpha = 0.5$. However, this parameter can vary substantially. An early paper by Nørskov *et al.* found a "universal α" of 0.84 for computed X–Y bond dissociation on flat transition metal surfaces.[90,197] For the Volmer reaction at Hg and Au electrodes with various proton donors and in various solvents, Conway, and Jackson and Surendranath, reported α values from 0.3 to 0.7,[206,207] which has recently been generalized.[208] Our kinetic studies of the hydrogen atom transfer from the CeO_xH_y nanoparticles in (Section VII.i) gave an α of 0.2 (over a 0.6 eV range).[163] The origins of these different α values are not clear. Even for well-defined homogenous, molecular HAT/PCET reactions, the large variation of α is an ongoing topic of research.[140,209-213]

IX. Volcano Plots with Broad Isotherms

Volcano plots have been discussed since Parsons and Gerischer's independent predictions in 1958[72,214] and early experimental tests by Conway and Bockris,[215] Ruetschi and Delahay,[216] and Trasatti.[217] In 2005, Nørskov and coworkers built a volcano plot from experimental rates and computed metal–H binding energies, using "a 2 × 2 surface cell …. [of] a three layer fcc(111) slab."[98] Calculations at hydrogen coverages of $\theta = ¼$ and $\theta = 1$ both gave clear volcano-shaped plots. That work has been extended in many directions.[27]

Most modern volcano plots have assumed regular surfaces and Langmuir isotherms, sometimes suggesting 'universal' relationships.[27,90,218-220] Still, the simplifications inherent in volcano plots have often been examined (*cf.*, [93,107,221,222]). In the context of this perspective, the variations among step edges, defects, and other surface heterogeneities can be highlighted. Different sites often have often have different BEP relations (different α and $k_0/\Delta G_0^{\ddagger}$, eqs 1, 2).[77,90,103,112,113,223,224] Thus, inhomogeneity and non-ideality should be relevant to volcano plots.

In his original paper, Parsons examined how the shape of a volcano plot for HER would change with a non-ideal isotherm for H binding.[72] He solved algebraically for the exchange current i_0 as a function of the standard state binding energy $\Delta G°$ (written as $\Delta g°$ in Figure 9). i_0 is the extrapolated current in each direction at zero driving force (similar to the j_0 above). The standard state was taken to be $\theta = ½$, and a Temkin isotherm was chosen for mathematical convenience. In this analysis, the different values of $\Delta g°$ implicitly refer to different catalysts that are "similar" in the ways discussed above. The conclusions were summarized with the text below (slightly edited) and the drawings in Figure 9.

> … the effect of assuming a Temkin isotherm on the curve of log(i_o) against $\Delta G°$ is to insert a horizontal region in the curve at its maximum as shown in fig. 8B…. Experimental studies of adsorption of gaseous hydrogen suggest that this horizontal section may be about 7 kcal mol^{-1} (0.3 eV) long.[72]

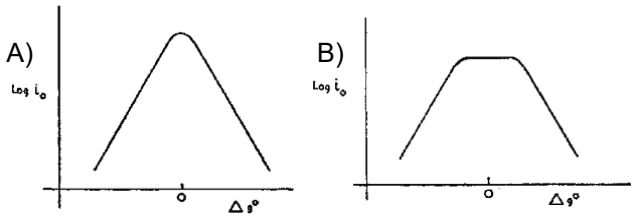

Figure 9. "Form of the relation between exchange current at a hydrogen electrode [log(i_0)] and the standard free energy of adsorption of hydrogen on the electrode surface [$\Delta G°_H$, labeled as $\Delta g°$], assuming that the adsorbed atoms (A) obey a Langmuir adsorption or (B) obey Temkin's logarithmic adsorption isotherm." Reproduced from *Trans. Faraday Soc.*, **1958**, *54*, 1053-1063; with permission from the Royal Society of Chemistry; permission conveyed through Copyright Clearance Center, Inc.

Parsons' estimation of a 7 kcal mol^{-1} (0.3 eV) width for the flat region in Figure 9B is a substantial fraction of the total width of a typical volcano plot. This conclusion is particularly significant when the flat section includes the expected Sabatier optimum. The width is roughly speaking the range of surface–H BDFEs, which is *ca.* 7 kcal mol^{-1} (0.3 eV) for a flat metal surface in contact with a gas or liquid phase. For instance, the width of just UPD-H binding on Pt(111) is about 0.3 eV (Figure 4), similar to the width for supported Pt nanoparticles + H_2(g).[74] The measured isotherm for H on CeO_2 nanoparticles is almost twice as wide. The wider and more irregular isotherms for more complex catalysts should give larger changes to the volcano shape. This insight from 1958 should be part of discussions in modern catalysis.

X. Case Study: H on cobalt phosphide and its volcano plot

i. Experiments and theory for CoP

Transition metal phosphides (TMPs) are being explored as substitutes for noble metals in reductive catalysis such as the HER.[225,226] TMPs are not simple materials, typically with multiple stoichiometries and structures. As stated by Cossairt and co-workers in their recent Perspective,[47]

> "The structural complexity of TMP surfaces introduces several H adsorption sites with varying [BDFEs]."[47]

The stoichiometric reaction of H_2 with cobalt phosphide (CoP)[225-227] has been explored.[228] Acid-washed, high surface area CoP adds hydrogen to give a highly hydrogenated material (ca. $CoP(H)_{0.3}$ *bulk* stoichiometry). Titrations with various molecular reagents showed the [CoP]–H UPD-H isotherm to be over 17 kcal mol^{-1} (0.7 eV) wide.

These experiments confirmed the results of a prior computational study of H on CoP.[229] That study found a variety of H adsorption sites, on various types of Co and P surface atoms, with occupancies and energies depending crystal face and coverage (Figure 10; panel e shows only the energies for H on the CoP(111) surface). In retrospect, the metal-oxide materials in Section VII are a simpler case because usually H binds only to oxygen.

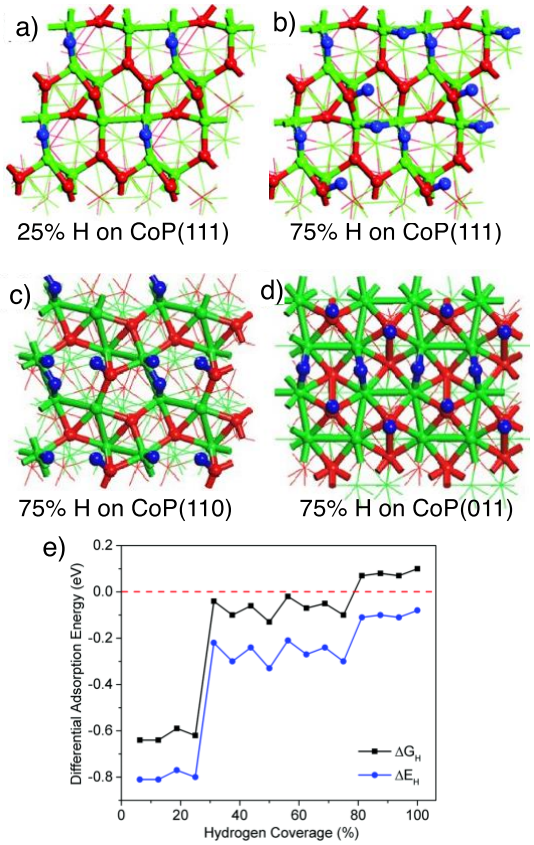

Figure 10. a)-d) Sites for H (blue balls) on various facets of CoP and different coverages, as indicated. Co = green; P = red. e) Differential adsorption energy (ΔE_H) and adsorption free energy (ΔG_H) as a function of hydrogen coverage on CoP(111) [BDFE = ΔG_H + 2.23 eV]. Reproduced from *Phys. Chem. Chem. Phys.*, **2008**, *10*, 3802-3811; [229] with permission from the Royal Society of Chemistry; permission conveyed through Copyright Clearance Center, Inc.

ii. CoP in the volcano plot for HER by transition metal phosphides

Figure 11 places the experimental isotherm as a burgundy-colored bar over the volcano plot developed for the HER by TMP. Additionally, the experiments do not probe the $\Delta G_H > 0$ region where binding energies are unfavorable. The computed isotherm in Figure 10e for the CoP(111) surface is similar to the experimental one.[229]

Nørskov and co-workers were well aware of the complexity of TMPs when they assembled this volcano plot, and they took an interesting approach to address this complexity. As detailed in their SI (edited for brevity with italics added):[230]

> [For] 2~5 surfaces of each TMP, the ΔG_H was calculated for hydrogen coverages from θ_H = 0 ML to 1 ML. Here, θ_H is defined as the fraction of a monolayer with respect to the number of active sites on the surface. The number of active sites on the surface is defined as number of possible sites where hydrogen can adsorb at a reasonable binding energy (ΔG_H < 0.7 eV). The coverage at which hydrogen desorption becomes more favorable than further adsorption is taken to be the coverage where HER occurs. *For each TMP, the surface with the most thermoneutral ΔG_H was considered to be the most active amongst the stable surfaces*; the ΔG_H at this surface is thus taken to be the descriptor for that TMP.[230]

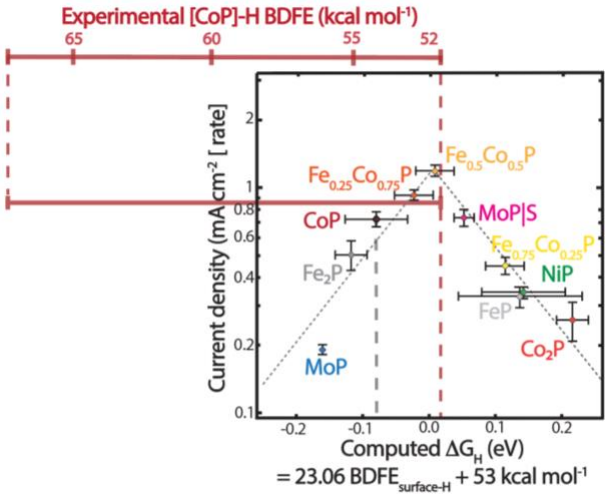

Figure 11. Composite image adapted and reprinted with permission from *J. Am. Chem. Soc.* **2023**, *145* (13), 7050-7064.[117] Copyright 2023 American Chemical Society. Experimental data (burgundy horizontal bars)[228] are plotted over a square plot of an activity volcano for the HER for TMPs, current density at η = 100 mV *vs.* computed ΔG_H (Reproduced from *Ener. Envir. Sci.* **2015**, *8* (10), 3022-3029,[230] with permission from the Royal Society of Chemistry; permission conveyed through Copyright Clearance Center, Inc.). The single ΔG_H shown for each material derive from a large set of computations.

The italics were added to the quote above to emphasize that this approach used the Sabatier Principle as the sole arbiter of which sites were most active. Likely this was chosen in part for computational convenience, but it seems to reflect the intuition of the field as well: only the $\Delta G°$ is relevant. This assumption was made even though it encompassed different active site structures. The points in Figure 11 include four active sites with H in P-atop sites, three with H in M-H-M bridge sites, and one with H in a three-fold metal hollow site, M_3H.[230] It goes against my inorganic chemist's intuition to correlate these sites with a single LFER, just because these sites have $\Delta G°_{H2}$ closest to 0 for their material.

As discussed in Section IV above, scaling relationships are required to simplify a traditional LFER with three parameters to an equation that depends only on $\Delta G°$.[27] For TMPs, a common scaling relation requires that the various PH and M_nH have the same reactivity when their $\Delta G°_H$ values are the same. I know of no precedent in molecular chemistry for such similarity between transition metal and non-metal compounds.

More generally, scaling relationships typically do not hold for more complex catalysts. An early computational study by Abild-Pedersen *et al.* showed that scaling relations for binding of EH_x fragments often differ by 0.5 eV or more between close-packed vs. stepped single crystal surfaces of the same element.[103] H adsorption on atop sites is ≥0.3 eV weaker than adsorption on the most stable site on the same transition-metal surface. This is one explanation for OPD and UPD-H on Pt(111) not falling on the same LFER. Greely later summarized the variability of scaling relationships:[113]

> These results imply that careful tuning of nanoparticle shape [of ideal transition metal crystals] could, in fact, change the scaling relationships and thus alter the optimal metal

> catalyst …. The structure sensitivity of the scaling relationships thus adds an extra dimension….[113]

While this manuscript was in revision, two papers were published that incorporated Frumkin isotherms into volcano plots for OER by cobalt oxide[31] and iridium oxide.[52] These studies built on prior experimental work (e.g., that in Section VII.iii[173]) and concluded (italics added):

> By combining predictions from density functional theory with parameters obtained from electroadsorption isotherms, we demonstrate that a destabilization of catalytic intermediates occurs with increasing coverage.[31]
>
> [The Frumkin isotherm] (~0.19 eV/monolayer) may account for a significant fraction of the observed OER catalytic activity in both [cobalt] materials."[31]
>
> … we present a modified volcano plot that elucidates how the intrinsic water oxidation kinetics can be increased by optimizing both the binding energy *and the interaction strength between the catalytically active states*.[52]

This Perspective generalizes these quotes to argue that understanding catalysis on complex surfaces requires more than the $\Delta G°$-based Sabatier optimum. Using LFERs requires at least some ability to sort the different sites, some measurements of the Brønsted α and $\Delta G_0^{\ddagger}$ parameters, and some knowledge of the isotherms for each site. When multiple distinct sites contribute to the catalysis, each site should probably have its own point on the volcano.

XI. Paths forward

The non-idealities of nanoscale interfaces presented here are not complexities to be avoided but rather opportunities for new advances in catalysis. This Perspective encourages the increasingly powerful experimental and computational tools in this field to be more frequently focused on the complexity of modern catalysts.

A central theme of this Perspective is that parameters other than the binding energy are important. Ideal LFER treatments and volcano plots using only $\Delta G°$ as a descriptor have been very valuable and impactful, but better models and intuition are needed for more complex catalysts.

That binding energies are not a sufficient descriptor is not a new conclusion. This has long been evident for single materials as "surface sensitivity."[112,231] Computational studies by Abild-Pedersen *et al.* showed the variety of scaling relationships for different types of single crystal metal surfaces almost 20 years ago.[103] Yet the Sabatier Principle is taken as the sole guide to catalytic activity in many current papers (though certainly not all). This Perspective aims to change that intuition.

i. Determining Isotherms and Kinetic Brønsted α's.

The quantitative hypothesis advanced here is that different sites follow different scaling relationships because of their variety of Brønsted αs and intrinsic barriers $\Delta G_0^{\ddagger}$ (eq 2).

The first step in testing this hypothesis—and in learning how to take advantage of site differentiation and non-idealities—is to directly measure the binding isotherms, αs and $\Delta G_0^{\ddagger}$s. This will require a focus on stoichiometric reactions of surfaces, in addition to overall catalytic metrics. There are some measurements and computations of this kind (*cf.*,[163,130,206-232]) but not yet enough to derive general principles. Studies of stoichiometric reactions of complex nanoparticles will in effect average over all of the variety sites on the surface. This will be a valuable complement to single-crystal studies.

Methods are increasingly available to measure isotherms, and this is made easier for nanoscale catalysts because of their high surface areas. Colloidal nanoparticles can often be studied by the classical equilibrium and kinetic methods of solution chemistry. Electrochemistry provides powerful and highly sensitive techniques to monitor adsorbates on electrodes (with care to distinguish faradaic from capacitive currents).[233,234] My laboratory is examining stoichiometric reactions with molecules in solution, as described above and in [235-240]. Measuring isotherms and rate constants at different coverages generate LFERs. The shape(s) and slope(s) of the LFER(s) should indicate the number of kinetically distinct sites within the isotherm, taking "similar" sites as those that fall on the same LFER.

Operando, *in situ*, and *ex situ* studies of reactive intermediates are increasingly common and are very informative. *Operando* measurements predominantly examine species that accumulate on a catalytic surface,[241] so some intermediates will need to be studied *ex situ*. Surface intermediates can likely be prepared using organic chemical approaches, as illustrated by the use of CH_3I in surface science to form surface methyl groups (*e.g.*, [242]). As one possible example, organic methods to deliver a formyl group[243] could perhaps form this important surface species and allow studies of its chemistry. Time-dependent applied potentials can also select different surface intermediates in favorable cases.[244,245]

Theory, computation, and experiment need to go hand-in-hand in characterizing adsorbate structures, energetics, and reactivity as a function of coverage. Complex, dynamic, non-stoichiometric surface structures can be challenging for theory, even to know where to start. Machine learning and related approaches are promising approaches to bridge the "complexity gap,"[56] and they will be helped by experimental datasets.

ii. "Seeing" the Surface: Spectroscopy, Microscopy, and other tools.

The characterization and study of surface intermediates is not a new quest, but it is increasingly accessible with the advent of increasingly powerful tools.[241,246] These include x-ray techniques; optical, vibrational, and other spectroscopies; electron microscopies and the expanding experiments that can be done in the microscope;[16,17] scanning probe microscopies; and high spatial resolution reactivity mapping.[38,247,248] Continuing challenges include connecting signal intensity with absolute surface coverages and identifying the kinetically competent vs. spectator species. Still, the future is exciting in this area.

Another issue is that most x-ray and electron tools are less sensitive to lighter atoms. The increased use of techniques sensitive to hydrogen and deuterium would be valuable, including TOF-SIMS, atom-probe tomography,[249] Rutherford back scattering,[250] and neutron experiments. Vibrational spectroscopy with isotopic substitution can be very powerful.[244] Still, the spectra can be overlapping, high frequency X–H stretching modes are not easily seen by

Raman and multidimensional techniques, and O–H and N–H modes are often broadened by hydrogen bonding. Still, great results are increasingly being obtained.[241] Imagine the insights that could be gained from an ability to characterize and quantitate $–CO_2H$, $–CH_2O$,–CHO, and/or $–CH_x$ groups on the surfaces of CO_2 reduction catalysts.

iii. Modeling Complex Isotherms

For surface diversity and non-ideality to become important parts of basic catalysis discussions, simple and accessible models are needed. Historically, there have been two limiting simplifications. One can assume that all the different sites behave similarly, can be treated as a Langmuir isotherm, and follow a single LFER. As noted above, this can be sufficient for traditional catalysts.[196] At the other extreme, the sites can be considered to be very different and only one type is catalytically active—Boudart's most abundant reactive intermediate (MARI).[114,115] Since modern catalysts are not well modelled by either limit, an intermediate model seems appropriate: approximating a broad and/or irregular isotherm as the sum of Langmuir isotherms (Scheme 4). Various multi-Langmuir models have long been used, for different applications (cf., [201,251-255]). As Wintterlin, Ertl, *et al.* wrote about NO dissociation on a Ru(0001) surface:[10]

> For "real" catalysis … the overall reactivity will be the result of weighted contributions from various surface structure elements, dominated by the active sites.[10]

Scheme 4. Modelling a Frumkin isotherm (blue) as the sum of three Langmuir isotherms (burgundy).

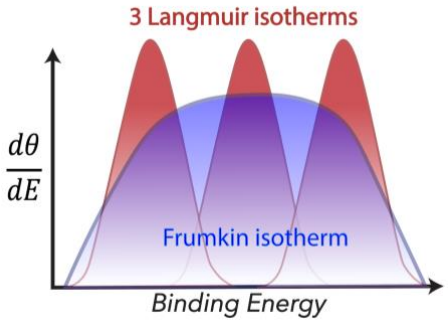

The multi-Langmuir model is intuitive when the broadness of the isotherm comes from distinct surface sites. Each component Langmuir isotherm is then treated as ideal, removing the complexities of non-ideal activities, rate 'constants', free energies, *etc.* Scheme 4 shows a Frumkin isotherm modeled as three ideal adsorbate states, each with its own coverage θ_i, saturation coverage $\theta_{i,max}$, standard free energy of adsorption, ΔG_i^o, and rate constant k_i.

On complex, ill-defined surfaces of nanoscale, multi-element catalysts, the surface structure elements and active sites are not known. Flipping the perspective of the quote above, the combination of a measured isotherm and catalytic activity as a function of surface could be a powerful way to analyze the surface elements and their activities.

Applying Scheme 4 to H on ceria NPs (Section VII.i), the separation of the three Langmuir isotherms would be ~6 kcal mol^{-1} (0.26 eV). With a Brønsted α of 0.5, this range of BDFEs would predict a variation in rate constants of ~10^4 between the outlying isotherms; with the experimental α = 0.2,[163] the range of k's among these groups is a factor of 15. As a more complex example, consider the Tafel reaction combining two surface H's (*H) to form H_2 (Figure 2 left). With one kind of *H well described by a single Langmuir isotherm, the rate law is simple second order (eq 20, with rapid surface diffusion). When there are i different sites, H_2 can be formed from two $*H_i$ or from different sites, $*H_i$ plus $*H_j$ (eq 21).[256,257] The latter mechanism was suggested for H_2 desorption from Mo_2NH_x: a hydridic Mo–$H^{\delta-}$ plus a protic N–$H^{\delta+}$.[198]

$$\frac{d[H_2]}{dt} = k(\theta_{*\mathrm{H}})^2 \quad (20)$$

$$\frac{d[H_2]}{dt} = \sum_i k_{ii}(\theta_{*H_i})^2 + \sum_{i,j} k_{ij}(\theta_{*H_i})(\theta_{*H_j}) \quad (21)$$

Electrochemical reaction steps can be similarly modeled, with multiple E_i^o analogous to the ΔG_i^o above. In a multi-Langmuir model, the Butler-Volmer equation (BV) becomes a sum of terms, each exponential in their $(E_{\mathrm{applied}} - E_i^o)$, and the current should not be simply exponential with potential. The presence of non-ideal isotherms is one likely reason why empirical Tafel slopes are typically not the integer multiples of (30 mV/decade)$^{-1}$ predicted by simple treatments.[258]

XII. Final thoughts

The increasing complexity of modern catalyst materials prompts a renewed emphasis on the non-ideal behavior of adsorbed catalytic intermediates. Compared to traditional metallic catalysts, nanoscale, multi-element, reactive catalysts often have a wide variety of surface sites, structures, stoichiometries, thermochemistry, adsorbate interactions, mechanisms, and reactivity. This diversity is a strength of these catalysts, a strength that should be harnessed to advance catalysis science and engineering.

Boudart's "three-step approach to surface kinetics" in *Kinetics on Ideal and Real Surfaces* (1956) included:[6]

> [In the] third step …. The nonideality of the surface process, including heterogeneity and interactions, must then be taken into account either by postulating a surface distribution of energy sites or by introducing real adsorption isotherms determined separately. While the third step … is hardly feasible in the vast majority of cases, there are a number of reasons for going beyond the first step whenever possible.

Now, 68 years later, it is time to tackle and take advantage of the non-ideality of complex catalysts.

ASSOCIATED CONTENT

There is no Supporting Information for this Perspective.

AUTHOR INFORMATION

Corresponding Author

* james.mayer@yale.edu
Department of Chemistry, Yale University, 225 Prospect St.,
New Haven CT 06520
Orchid ID: 0000-0002-3943-5250

FUNDING SOURCES

Financial support from the following sources is gratefully acknowledged (the research topic(s) funded by each program are stated). The Center for Molecular Electrocatalysis (CME), an Energy Frontier Research Center funded by the U.S. Department of Energy, Office of Science, Office of Basic Energy Sciences: CoP and NiO. A Swiss National Science Foundation (SNSF) PRIMA postdoctoral fellowship to Prof. Murielle Delley provided partial support for CoP studies. The National Science Foundation: ZnO, TiO_2, and CeO_2 in aprotic solvents (CHE-1151726, CHE-1609434 and CHE-1904813, and through graduate research fellowships). The Department of Energy, Basic Energy Sciences, Catalysis program (Award # DE-SC0021298): aqueous TiO_2 and IrO_2. The US/Israel Bilateral Science Foundation: aqueous TiO_2. The Multidisciplinary Research Program of the University Research Initiative (MURI) "Molecular-Scale Studies of Liquid−Solid Interfaces in Electrochemical Processes," supported by the Air Force Office of Scientific Research under award number FA9550-18-1-0420: Pt and Au. The Center for Hybrid Approaches in Solar Energy to Liquid Fuels (CHASE), an Energy Innovation Hub funded by the U.S. Department of Energy, Office of Science, Office of Basic Energy Sciences under Award Number DE-SC0021173 (Si).

ACKNOWLEDGMENTS

This Perspective has been stimulated by intellectual and experimental contributions from many students, postdocs, collaborators, and friends, especially through the multi-PI programs listed above. I am grateful for the insights and research of Prof. Murielle Delley (CoP), Dr. Rishi G. Agarwal (ceria), Prof. Hyunho Noh (NiO), Prof. Robert Warburton (TiO_2), and Dr. Nicolas Dwarica, Dr. Peter Rice, and Dr. Simone Raugei (Fe_xC). In various discussions, Profs. Hector Abrũna, Jason Bates, Brandi Cossairt, James McKone, and Yogi Surendranath have tried to keep the author from going too far off the rails. E. Stewart-Jones and K. Rinaolo are thanked for drafting some of the Figures and Schemes.

TOC GRAPHIC

Volcano plot for HER by transition metal phosphides with experimental values for CoP
recast from *J. Am. Chem. Soc.* **2023**, *145*, 7050-7064,

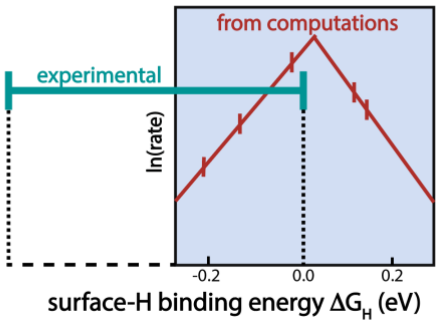

References

(1) Ertl, G. Thermo-chemical kinetic profile of ammonia synthesis on iron catalysts. *Catal. Rev. Sci. Eng* **1980**, *21*, 201-223. DOI: 10.1080/03602458008067533.

(2) Wintterlin, J.; Völkening, S.; Janssens, T. V. W.; Zambelli, T.; Ertl, G. Atomic and Macroscopic Reaction Rates of a Surface-Catalyzed Reaction. *Science* **1997**, *278* (5345), 1931-1934. DOI: 10.1126/science.278.5345.1931.

(3) Boudart, M.; Djega-Mariadassou, G. *Kinetics of Heterogeneous Catalytic Reactions*; Princeton University Press, 1984. DOI: doi:10.1515/9781400853335.

(4) Xu, Z.; Kitchin, J. R. Probing the Coverage Dependence of Site and Adsorbate Configurational Correlations on (111) Surfaces of Late Transition Metals. *The Journal of Physical Chemistry C* **2014**, *118* (44), 25597-25602. DOI: 10.1021/jp508805h.

(5) Bhandari, S.; Rangarajan, S.; Maravelias, C. T.; Dumesic, J. A.; Mavrikakis, M. Reaction Mechanism of Vapor-Phase Formic Acid Decomposition over Platinum Catalysts: DFT, Reaction Kinetics Experiments, and Microkinetic Modeling. *ACS Catalysis* **2020**, *10* (7), 4112-4126. DOI: 10.1021/acscatal.9b05424.

(6) Boudart, M. Kinetics on ideal and real surfaces. *AlChE J.* **1956**, *2* (1), 62-64. DOI: 10.1002/aic.690020113.

(7) Boudart, M.; Djega-Mariadassou, G. Chapter 4: Kinetics of two-step reactions on non-uniform surfaces. In *Kinetics of Heterogeneous Catalytic Reactions;*, Princeton University Press, 1984; pp 118-154.

(8) Somorjai, G. A.; Li, Y. *Introduction to Surface Chemistry and Catalysis*; John Wiley & Sons, 2010; quote is from p. 317.

(9) Van Hardeveld, R.; Hartog, F. The statistics of surface atoms and surface sites on metal crystals. *Surf. Sci.* **1969**, *15* (2), 189-230. DOI: 10.1016/0039-6028(69)90148-4.

(10) Zambelli, T.; Wintterlin, J.; Trost, J.; Ertl, G. Identification of the "Active Sites" of a Surface-Catalyzed Reaction. *Science* **1996**, *273* (5282), 1688-1690. DOI: 10.1126/science.273.5282.1688.

(11) Sinfelt, J. H. Catalysis by alloys and bimetallic clusters. *Acc. Chem. Res.* **1977**, *10* (1), 15-20. DOI: 10.1021/ar50109a003.

(12) Somorjai, G. A. Surface Reconstruction and Catalysis. *Annu. Rev. Phys. Chem.* **1994**, *45* (1), 721-751. DOI: 10.1146/annurev.pc.45.100194.003445.

(13) Timoshenko, J.; Roldan Cuenya, B. In Situ/Operando Electrocatalyst Characterization by X-ray Absorption Spectroscopy. *Chem. Rev.* **2021**, *121* (2), 882-961. DOI: 10.1021/acs.chemrev.0c00396.

(14) Li, Y.; Zakharov, D.; Zhao, S.; Tappero, R.; Jung, U.; Elsen, A.; Baumann, P.; Nuzzo, R. G.; Stach, E. A.; Frenkel, A. I. Complex structural dynamics of nanocatalysts revealed in Operando conditions by correlated imaging and spectroscopy probes. *Nature Communications* **2015**, *6* (1), 7583. DOI: 10.1038/ncomms8583.

(15) Nguyen, Q. N.; Chen, R.; Xia, Y. Shape-controlled synthesis of metal nanocrystals: mind the surface heterogeneity. *Trends in Chemistry* **2023**, *5* (10), 748-762. DOI: 10.1016/j.trechm.2023.08.004.

(16) Chee, S. W.; Lunkenbein, T.; Schlögl, R.; Roldán Cuenya, B. Operando Electron Microscopy of Catalysts: The Missing Cornerstone in Heterogeneous Catalysis Research? *Chem. Rev.* **2023**. DOI: 10.1021/acs.chemrev.3c00352.

(17) Cao, K.; Zoberbier, T.; Biskupek, J.; Botos, A.; McSweeney, R. L.; Kurtoglu, A.; Stoppiello, C. T.; Markevich, A. V.; Besley, E.; Chamberlain, T. W.; et al. Comparison of atomic scale dynamics for the middle and late transition metal nanocatalysts. *Nature Communications* **2018**, *9* (1), 3382. DOI: 10.1038/s41467-018-05831-z.

(18) Bullock, R. M.; Chen, J. G.; Gagliardi, L.; Chirik, P. J.; Farha, O. K.; Hendon, C. H.; Jones, C. W.; Keith, J. A.; Klosin, J.; Minteer, S. D.; et al. Using nature's blueprint to expand catalysis with Earth-abundant metals. *Science* **2020**, *369* (6505), eabc3183. DOI: 10.1126/science.abc3183.

(19) Liu, Y.; McCue, A. J.; Li, D. Metal Phosphides and Sulfides in Heterogeneous Catalysis: Electronic and Geometric Effects. *ACS Catalysis* **2021**, *11* (15), 9102-9127. DOI: 10.1021/acscatal.1c01718.

(20) Lin, Z.; Denny, S. R.; Chen, J. G. Transition metal carbides and nitrides as catalysts for thermochemical reactions. *J. Catal.* **2021**, *404*, 929-942. DOI: 10.1016/j.jcat.2021.06.022.

(21) Vedrine, J. C. Metal Oxides in Heterogeneous Catalysis; Elsevier, 2018.

(22) Kawashima, K.; Márquez, R. A.; Smith, L. A.; Vaidyula, R. R.; Carrasco-Jaim, O. A.; Wang, Z.; Son, Y. J.; Cao, C. L.; Mullins, C. B. A Review of Transition Metal Boride, Carbide, Pnictide, and Chalcogenide Water Oxidation Electrocatalysts. *Chem. Rev.* **2023**, 123, 23, 12795–13208 DOI: 10.1021/acs.chemrev.3c00005.

(23) Mitchell, J. B.; Chagnot, M.; Augustyn, V. Hydrous Transition Metal Oxides for Electrochemical Energy and Environmental Applications. *Annu. Rev. Mater. Res.* **2023**, *53* (1), 1-23. DOI: 10.1146/annurev-matsci-080819-124955.

(24) Pfeifer, V.; Jones, T. E.; Wrabetz, S.; Massue, C.; Velasco Velez, J. J.; Arrigo, R.; Scherzer, M.; Piccinin, S.; Havecker, M.; Knop-Gericke, A.; et al. Reactive oxygen species in iridium-based OER catalysts. *Chem. Sci.* **2016**, *7* (11), 6791-6795. DOI: 10.1039/c6sc01860b.

(25) Mom, R. V.; Falling, L. J.; Kasian, O.; Algara-Siller, G.; Teschner, D.; Crabtree, R. H.; Knop-Gericke, A.; Mayrhofer, K. J. J.; Velasco-Vélez, J.-J.; Jones, T. E. Operando Structure–Activity–Stability Relationship of Iridium Oxides during the Oxygen Evolution Reaction. *ACS Catalysis* **2022**, *12* (9), 5174-5184. DOI: 10.1021/acscatal.1c05951.

(26) Willinger, E.; Massué, C.; Schlögl, R.; Willinger, M. G. Identifying Key Structural Features of IrO_x Water Splitting Catalysts. *Journal of the American Chemical Society* **2017**, *139* (34), 12093-12101. DOI: 10.1021/jacs.7b07079.

(27) Medford, A. J.; Vojvodic, A.; Hummelshøj, J. S.; Voss, J.; Abild-Pedersen, F.; Studt, F.; Bligaard, T.; Nilsson, A.; Nørskov, J. K. From the Sabatier principle to a predictive theory of transition-metal heterogeneous catalysis. *J. Catal.* **2015**, *328*, 36-42. DOI: 10.1016/j.jcat.2014.12.033.

(28) Goswami, A.; Ma, H.; Schneider, W. F. Consequences of adsorbate-adsorbate interactions for apparent kinetics of surface catalytic reactions. *J. Catal.* **2022**, *405*, 410-418. DOI: 10.1016/j.jcat.2021.12.005.

(29) Miller, S.; Dsilva, C.; Kitchin, J. R. Coverage dependent adsorption properties of atomic adsorbates on late transition metal surfaces. In *Catalysis*, Spivey, J. J., Gupta, M. Eds.; Vol. 24; The Royal Society of Chemistry, 2012; p 83 - 115.

(30) Reuter, K.; Plaisance, C. P.; Oberhofer, H.; Andersen, M. Perspective: On the active site model in computational catalyst screening. *The Journal of Chemical Physics* **2017**, *146* (4), 040901. DOI: 10.1063/1.4974931.

(31) Moss, B.; Svane, K. L.; Nieto-Castro, D.; Rao, R. R.; Scott, S. B.; Tseng, C.; Sachs, M.; Pennathur, A.; Liang, C.; Oldham, L. I.; et al. Cooperative Effects Drive Water Oxidation Catalysis in Cobalt Electrocatalysts through the

Destabilization of Intermediates. *Journal of the American Chemical Society* **2024**, *146* (13), 8915-8927. DOI: 10.1021/jacs.3c11651.

(32) Kuo, D.-Y.; Paik, H.; Kloppenburg, J.; Faeth, B.; Shen, K. M.; Schlom, D. G.; Hautier, G.; Suntivich, J. Measurements of Oxygen Electroadsorption Energies and Oxygen Evolution Reaction on RuO_2(110): A Discussion of the Sabatier Principle and Its Role in Electrocatalysis. *Journal of the American Chemical Society* **2018**, *140* (50), 17597-17605. DOI: 10.1021/jacs.8b09657.

(33) Jung, O.; Jackson, M. N.; Bisbey, R. P.; Kogan, N. E.; Surendranath, Y. Innocent buffers reveal the intrinsic pH- and coverage-dependent kinetics of the hydrogen evolution reaction on noble metals. *Joule* **2022**, *6* (2), 476-493. DOI: 10.1016/j.joule.2022.01.007.

(34) Chen, Z.; Liu, Z.; Xu, X. Coverage-Dependent Microkinetics in Heterogeneous Catalysis Powered by the Maximum Rate Analysis. *ACS Catalysis* **2021**, *11* (15), 9333-9344. DOI: 10.1021/acscatal.1c01997.

(35) Lucky, C.; Schreier, M. Mind the Interface: The Role of Adsorption in Electrocatalysis. *ACS Nano* **2024**, *18* (8), 6008-6015. DOI: 10.1021/acsnano.3c09523.

(36) Ishida, T.; Murayama, T.; Taketoshi, A.; Haruta, M. Importance of Size and Contact Structure of Gold Nanoparticles for the Genesis of Unique Catalytic Processes. *Chem. Rev.* **2020**, *120* (2), 464-525. DOI: 10.1021/acs.chemrev.9b00551.

(37) Rommens, K. T.; Saeys, M. Molecular Views on Fischer–Tropsch Synthesis. *Chem. Rev.* **2023**, *123* (9), 5798-5858. DOI: 10.1021/acs.chemrev.2c00508.

(38) Carvalho, O. Q.; Adiga, P.; Murthy, S. K.; Fulton, J. L.; Gutierrez, O. Y.; Stoerzinger, K. A. Understanding the Role of Surface Heterogeneities in Electrosynthesis Reactions. *iScience* **2020**, *23* (12), 101814. DOI: 10.1016/j.isci.2020.101814.

(39) Dones Lassalle, C. Y.; Kelm, J. E.; Dempsey, J. L. Characterizing the Semiconductor Nanocrystal Surface through Chemical Reactivity. *Acc. Chem. Res.* **2023**, *56* (13), 1744-1755. DOI: 10.1021/acs.accounts.3c00125.

(40) Kessler, M. L.; Dempsey, J. L. Mapping the Topology of PbS Nanocrystals through Displacement Isotherms of Surface-Bound Metal Oleate Complexes. *Chemistry of Materials* **2020**, *32* (6), 2561-2571. DOI: 10.1021/acs.chemmater.0c00014.

(41) Saniepay, M.; Mi, C.; Liu, Z.; Abel, E. P.; Beaulac, R. Insights into the Structural Complexity of Colloidal CdSe Nanocrystal Surfaces: Correlating the Efficiency of Nonradiative Excited-State Processes to Specific Defects. *Journal of the American Chemical Society* **2018**, *140* (5), 1725-1736. DOI: 10.1021/jacs.7b10649.

(42) Dümbgen, K. C.; Infante, I.; Hens, Z. Localizing Oleylamine Ligands on Amine–Halide Copassivated Indium Phosphide Nanocrystals. *Chemistry of Materials* **2023**, *35* (11), 4393-4403. DOI: 10.1021/acs.chemmater.3c00565.

(43) Green, P. B.; Yarur Villanueva, F.; Imperiale, C. J.; Hasham, M.; Demmans, K. Z.; Burns, D. C.; Wilson, M. W. B. Directed Ligand Exchange on the Surface of PbS Nanocrystals: Implications for Incoherent Photon Conversion. *ACS Applied Nano Materials* **2021**, *4* (6), 5655-5664. DOI: 10.1021/acsanm.1c00853.

(44) Prather, K. V.; Stoffel, J. T.; Tsui, E. Y. Z-Type Ligand Coordination at Colloidal Semiconductor Nanocrystals Modifies Surface Electrostatics. *Chemistry of Materials* **2022**, *34* (9), 3976-3984. DOI: 10.1021/acs.chemmater.1c04439.

(45) Brewer, A. S.; Calvin, J. J.; Alivisatos, A. P. Impact of Uniform Facets on the Thermodynamics of Ligand Exchanges on Colloidal Quantum Dots. *The Journal of Physical Chemistry C* **2023**, *127* (21), 10270-10281. DOI: 10.1021/acs.jpcc.3c00187.

(46) Meyer, H. M.; Chen, J.; Loomis, R. A.; Buhro, W. E. Facet-Specific Electron Transfer in Pseudo-Two-Dimensional Wurtzite Cadmium Selenide Nanocrystals. *The Journal of Physical Chemistry C* **2023**, *127* (37), 18506-18517. DOI: 10.1021/acs.jpcc.3c03825.

(47) Kuo, D.-Y.; Nishiwaki, E.; Rivera-Maldonado, R. A.; Cossairt, B. M. The Role of Hydrogen Adsorption Site Diversity in Catalysis on Transition-Metal Phosphide Surfaces. *ACS Catalysis* **2023**, *13* (1), 287-295. DOI: 10.1021/acscatal.2c04936.

(48) Skúlason, E.; Tripkovic, V.; Björketun, M. E.; Gudmundsdóttir, S.; Karlberg, G.; Rossmeisl, J.; Bligaard, T.; Jónsson, H.; Nørskov, J. K. Modeling the Electrochemical Hydrogen Oxidation and Evolution Reactions on the Basis of Density Functional Theory Calculations. *The Journal of Physical Chemistry C* **2010**, *114* (42), 18182-18197. DOI: 10.1021/jp1048887.

(49) Goswami, A.; Schneider, W. F. Mean field model parameterization to recover coverage-dependent kinetics. *J. Catal.* **2023**, *426*, 352-360. DOI: 10.1016/j.jcat.2023.07.013

(50) Deimel, M.; Reuter, K.; Andersen, M. Active Site Representation in First-Principles Microkinetic Models: Data-Enhanced Computational Screening for Improved Methanation Catalysts. *ACS Catalysis* **2020**, *10* (22), 13729-13736. DOI: 10.1021/acscatal.0c04045.

(51) Ma, H.; Schneider, W. F. DFT and microkinetic comparison of Pt, Pd and Rh-catalyzed ammonia oxidation. *J. Catal.* **2020**, *383*, 322-330. DOI: 10.1016/j.jcat.2020.01.029.

(52) Liang, C.; Rao, R. R.; Svane, K. L.; Hadden, J. H. L.; Moss, B.; Scott, S. B.; Sachs, M.; Murawski, J.; Frandsen, A. M.; Riley, D. J.; et al. Unravelling the effects of active site density and energetics on the water oxidation activity of iridium oxides. *Nat. Catal.* **2024**, *7* (7), 763-775. DOI: 10.1038/s41929-024-01168-7.

(53) Razdan, N. K.; Bhan, A. Kinetic description of site ensembles on catalytic surfaces. *Proceedings of the National Academy of Sciences* **2021**, *118* (8), e2019055118. DOI: 10.1073/pnas.2019055118.

(54) Razdan, N. K.; Lin, T. C.; Bhan, A. Concepts Relevant for the Kinetic Analysis of Reversible Reaction Systems. *Chem. Rev.* **2023**, *123* (6), 2950-3006. DOI: 10.1021/acs.chemrev.2c00510.

(55) van der Stam, W. The Necessity for Multiscale In Situ Characterization of Tailored Electrocatalyst Nanoparticle Stability. *Chemistry of Materials* **2023**, *35* (2), 386-394. DOI: 10.1021/acs.chemmater.2c03286.

(56) Mou, T.; Pillai, H. S.; Wang, S.; Wan, M.; Han, X.; Schweitzer, N. M.; Che, F.; Xin, H. Bridging the complexity gap in computational heterogeneous catalysis with machine learning. *Nat. Catal.* **2023**, *6* (2), 122-136. DOI: 10.1038/s41929-023-00911-w.

(57) Trindell, J. A.; Duan, Z.; Henkelman, G.; Crooks, R. M. Well-Defined Nanoparticle Electrocatalysts for the Refinement of Theory. *Chem. Rev.* **2020**, *120* (2), 814-850. DOI: 10.1021/acs.chemrev.9b00246.

(58) Yeh, A. H.-W.; Norn, C.; Kipnis, Y.; Tischer, D.; Pellock, S. J.; Evans, D.; Ma, P.; Lee, G. R.; Zhang, J. Z.; Anishchenko, I.; et al. De novo design of luciferases using deep learning. *Nature* **2023**, *614* (7949), 774-780. DOI: 10.1038/s41586-023-05696-3.

(59) Nguyen, T. N.; Nhat, T. T. P.; Takimoto, K.; Thakur, A.; Nishimura, S.; Ohyama, J.; Miyazato, I.; Takahashi, L.; Fujima, J.; Takahashi, K.; et al. High-Throughput Experimentation and Catalyst Informatics for Oxidative Coupling of Methane. *ACS Catalysis* **2020**, *10* (2), 921-932. DOI: 10.1021/acscatal.9b04293.

(60) Roy, D.; Mandal, S. C.; Pathak, B. Machine Learning-Driven High-Throughput Screening of Alloy-Based Catalysts for Selective CO2 Hydrogenation to Methanol. *ACS Appl. Mater. Interfaces* **2021**, *13* (47), 56151-56163. DOI: 10.1021/acsami.1c16696.

(61) Steinmann, S. N.; Hermawan, A.; Bin Jassar, M.; Seh, Z. W. Autonomous high-throughput computations in catalysis. *Chem Catalysis* **2022**, *2* (5), 940-956. DOI: 0.1016/j.checat.2022.02.009.

(62) Newman-Stonebraker Samuel, H.; Smith Sleight, R.; Borowski Julia, E.; Peters, E.; Gensch, T.; Johnson Heather, C.; Sigman Matthew, S.; Doyle Abigail, G. Univariate classification of phosphine ligation state and reactivity in cross-coupling catalysis. *Science* **2021**, *374* (6565), 301-308. DOI: 10.1126/science.abj4213 (acccessed 2021/10/15).

(63) Allen, C. L.; Leitch, D. C.; Anson, M. S.; Zajac, M. A. The power and accessibility of high-throughput methods for catalysis research. *Nat. Catal.* **2019**, *2* (1), 2-4. DOI: 10.1038/s41929-018-0220-4.

(64) Nieuwelink, A.-E.; Vollenbroek, J. C.; Tiggelaar, R. M.; Bomer, J. G.; van den Berg, A.; Odijk, M.; Weckhuysen, B. M. High-throughput activity screening and sorting of single catalyst particles with a droplet microreactor using dielectrophoresis. *Nat. Catal.* **2021**, *4* (12), 1070-1079. DOI: 10.1038/s41929-021-00718-7.

(65) Martindale, B.; Völler, J.-S.; Capdevila-Cortada, M.; Editors. Machine Learning in Catalysis (online collection). *Nat. Catal.* **2023**.

(66) Musa, E.; Doherty, F.; Goldsmith, B. R. Accelerating the structure search of catalysts with machine learning. *Current Opinion in Chemical Engineering* **2022**, *35*, 100771. DOI: 10.1016/j.coche.2021.100771.

(67) Green, M. L. H. A new approach to the formal classification of covalent compounds of the elements. *J. Organomet. Chem.* **1995**, *500* (1), 127-148. DOI: 10.1016/0022-328X(95)00508-N.

(68) Green, M. L. H.; Parkin, G. Application of the Covalent Bond Classification Method for the Teaching of Inorganic Chemistry. *Journal of Chemical Education* **2014**, *91* (6), 807-816. DOI: 10.1021/ed400504f.

(69) Owen, J. The coordination chemistry of nanocrystal surfaces. *Science* **2015**, *347* (6222), 615-616. DOI: 10.1126/science.1259924 (acccessed 2023/08/06).

(70) Parshall, G. W.; Ittel, S. D. Homogeneous Catalysis: The Applications and Chemistry of Catalysis by Soluble Transition Metal Complexes; Wiley-Interscience, 1992.

(71) Ayawei, N.; Ebelegi, A. N.; Wankasi, D. Modelling and Interpretation of Adsorption Isotherms. *Journal of Chemistry* **2017**, *2017*, 3039817. DOI: 10.1155/2017/3039817.

(72) Parsons, R. The rate of electrolytic hydrogen evolution and the heat of adsorption of hydrogen. *Trans. Faraday Soc.* **1958**, *54*, 1053-1063. DOI: 10.1039/TF9585401053.

(73) Conway, B. E.; Angerstein-Kozlowska, H. The electrochemical study of multiple-state adsorption in monolayers. *Acc. Chem. Res.* **1981**, *14* (2), 49-56. DOI: 10.1021/ar00062a004.

(74) García-Diéguez, M.; Hibbitts, D. D.; Iglesia, E. Hydrogen Chemisorption Isotherms on Platinum Particles at Catalytic Temperatures: Langmuir and Two-Dimensional Gas Models Revisited. *The Journal of Physical Chemistry C* **2019**, *123* (13), 8447-8462. DOI: 10.1021/acs.jpcc.8b10877.

(75) Climent, V.; Feliu, J. M. Thirty years of platinum single crystal electrochemistry. *J. Solid State Electrochem.* **2011**, *15* (7), 1297-1315. DOI: 10.1007/s10008-011-1372-1.

(76) Boudart, M.; Djega-Mariadassou, G. Chapter 5: Struture-Insensitive and Structure-Sensitive Reactions on Metals. In *Kinetics of Heterogeneous Catalytic Reactions;*, Princeton University Press, 1984; pp 155-193.

(77) Rizo, R.; Fernández-Vidal, J.; Hardwick, L. J.; Attard, G. A.; Vidal-Iglesias, F. J.; Climent, V.; Herrero, E.; Feliu, J. M. Investigating the presence of adsorbed species on Pt steps at low potentials. *Nature Communications* **2022**, *13* (1), 2550. DOI: 10.1038/s41467-022-30241-7.

(78) McCrum, I. T.; Bondue, C. J.; Koper, M. T. M. Hydrogen-Induced Step-Edge Roughening of Platinum Electrode Surfaces. *The Journal of Physical Chemistry Letters* **2019**, *10* (21), 6842-6849. DOI: 10.1021/acs.jpclett.9b02544.

(79) Wang, J. X.; Markovic, N. M.; Adzic, R. R. Kinetic Analysis of Oxygen Reduction on Pt(111) in Acid Solutions: Intrinsic Kinetic Parameters and Anion Adsorption Effects. *The Journal of Physical Chemistry B* **2004**, *108* (13), 4127-4133. DOI: 10.1021/jp037593v.

(80) Lebedeva, N. P.; Koper, M. T. M.; Feliu, J. M.; van Santen, R. A. Role of Crystalline Defects in Electrocatalysis: Mechanism and Kinetics of CO Adlayer Oxidation on Stepped Platinum Electrodes. *The Journal of Physical Chemistry B* **2002**, *106* (50), 12938-12947. DOI: 10.1021/jp0204105.

(81) Somorjai, G. A.; Carrazza, J. Structure sensitivity of catalytic reactions. *Industrial & engineering chemistry fundamentals* **1986**, *25* (1), 63-69.

(82) Koper, M. T. M. Structure sensitivity and nanoscale effects in electrocatalysis. *Nanoscale* **2011**, *3* (5), 2054-2073. DOI: 10.1039/C0NR00857E.

(83) Sabatier, P. *La catalyse en chimie organique*; C. Béranger, 1920.

(84) Ooka, H.; Huang, J.; Exner, K. S. The Sabatier Principle in Electrocatalysis: Basics, Limitations, and Extensions. *Frontiers in Energy Research* **2021**, *9*, 155. DOI: 10.3389/fenrg.2021.654460.

(85) Che, M. Nobel Prize in chemistry 1912 to Sabatier: Organic chemistry or catalysis? *Catalysis Today* **2013**, *218-219*, 162-171. DOI: 10.1016/j.cattod.2013.07.006.

(86) Gileadi, E. Chapter 19: Adsorption isotherms for intermediates formed by charge transfer. In *Electrode Kinetics for Chemists, Chemical Engineers and Materials Scientists*, VCH Publishers, 1993; pp 261-280.

(87) Schmickler, W.; Santos, E. Chapter 6: Adsorption on metal electrodes: principles; Chapter 14: Hydrogen reaction and electrocatalysis. In *Interfacial Electrochemistry*, 2nd ed.; Springer-Verlag, 2010; pp 51-65 and 163-175.

(88) Jencks, W. P. A primer for the Bema Hapothle. An empirical approach to the characterization of changing transition-state structures. *Chem. Rev.* **1985**, *85* (6), 511-527. DOI: 10.1021/cr00070a001.

(89) van Santen, R. A.; Neurock, M.; Shetty, S. G. Reactivity Theory of Transition-Metal Surfaces: A Brønsted−Evans−Polanyi Linear Activation Energy−Free-Energy Analysis. *Chem. Rev.* **2010**, *110* (4), 2005 - 2048. DOI: 10.1021/cr9001808.

(90) Wang, S.; Temel, B.; Shen, J.; Jones, G.; Grabow, L. C.; Studt, F.; Bligaard, T.; Abild-Pedersen, F.; Christensen, C. H.; Nørskov, J. K. Universal Brønsted-Evans-Polanyi Relations for C–C, C–O, C–N, N–O, N–N, and O–O Dissociation Reactions. *Catal. Lett.* **2011**, *141* (3), 370-373. DOI: 10.1007/s10562-010-0477-y.

(91) Bligaard, T.; Nørskov, J. K.; Dahl, S.; Matthiesen, J.; Christensen, C. H.; Sehested, J. The Brønsted–Evans–Polanyi relation and the volcano curve in heterogeneous catalysis. *J. Catal.* **2004**, *224* (1), 206-217. DOI: 10.1016/j.jcat.2004.02.034.

(92) Akhade, S. A.; Nidzyn, R. M.; Rostamikia, G.; Janik, M. J. Using Brønsted-Evans-Polanyi relations to predict electrode potential-dependent activation energies. *Catalysis Today* **2018**, *312*, 82-91. DOI: 10.1016/j.cattod.2018.03.048.

(93) Lindgren, P.; Kastlunger, G.; Peterson, A. A. A Challenge to the G ∼ 0 Interpretation of Hydrogen Evolution. *ACS Catalysis* **2020**, *10* (1), 121-128. DOI: 10.1021/acscatal.9b02799.

(94) Gileadi, E. Chapter F14: Multi Step Electrode Reactions: Mechanistic Criteria. In *Electrode Kinetics for Chemists, Chemical Engineers and Materials Scientists*, VCH Publishers, 1993; pp 127-161.

(95) Pegis, M. L.; Wise, C. F.; Koronkiewicz, B.; Mayer, J. M. Identifying and Breaking Scaling Relations in Molecular Catalysis of Electrochemical Reactions. *Journal of the American Chemical Society* **2017**, *139* (32), 11000-11003. DOI: 10.1021/jacs.7b05642.

(96) Martin, D. J.; Wise, C. F.; Pegis, M. L.; Mayer, J. M. Developing Scaling Relationships for Molecular Electrocatalysis through Studies of Fe-Porphyrin-Catalyzed O_2 Reduction. *Acc. Chem. Res.* **2020**, *53* (5), 1056-1065. DOI: 10.1021/acs.accounts.0c00044.

(97) Cheng, J.; Hu, P.; Ellis, P.; French, S.; Kelly, G.; Lok, C. M. Brønsted−Evans−Polanyi Relation of Multistep Reactions and Volcano Curve in Heterogeneous Catalysis. *The Journal of Physical Chemistry C* **2008**, *112* (5), 1308-1311. DOI: 10.1021/jp711191j.

(98) Nørskov, J. K.; Bligaard, T.; Logadottir, A.; Kitchin, J. R.; Chen, J. G.; Pandelov, S.; Stimming, U. Trends in the Exchange Current for Hydrogen Evolution. *Journal of the Electrochemical Society* **2005**, *152* (3), J23. DOI: 10.1149/1.1856988.

(99) Campbell, C. T. The Degree of Rate Control: A Powerful Tool for Catalysis Research. *ACS Catalysis* **2017**, *7* (4), 2770-2779. DOI: 10.1021/acscatal.7b00115.

(100) Greeley, J. Theoretical Heterogeneous Catalysis: Scaling Relationships and Computational Catalyst Design. *Annual Review of Chemical and Biomolecular Engineering* **2016**, *7* (1), 605-635. DOI: 10.1146/annurev-chembioeng-080615-034413.

(101) Motagamwala, A. H.; Dumesic, J. A. Microkinetic Modeling: A Tool for Rational Catalyst Design. *Chem. Rev.* **2021**, *121* (2), 1049-1076. DOI: 10.1021/acs.chemrev.0c00394.

(102) Kozuch, S.; Shaik, S. A Combined Kinetic−Quantum Mechanical Model for Assessment of Catalytic Cycles: Application to Cross-Coupling and Heck Reactions. *Journal of the American Chemical Society* **2006**, *128* (10), 3355-3365. DOI: 10.1021/ja0559146.

(103) Abild-Pedersen, F.; Greeley, J.; Studt, F.; Rossmeisl, J.; Munter, T. R.; Moses, P. G.; Skúlason, E.; Bligaard, T.; Nørskov, J. K. Scaling Properties of Adsorption Energies for Hydrogen-Containing Molecules on Transition-Metal Surfaces. *Phys. Rev. Lett.* **2007**, *99* (1), 016105. DOI: 10.1103/PhysRevLett.99.016105.

(104) Gerischer, H. Über den Zusammenhang zwischen dem Mechanismus der elektrolytischen Wasserstoffabscheidung und der Adsorptionsenergie des atomaren Wasserstoffs an verschiedenen Metallen. **1956**, *8* (3-4), 137-153. DOI: 10.1524/zpch.1956.8.3_4.137.

(105) Trasatti, S. Electronegativity, work function, and heat of adsorption of hydrogen on metals. *J. Chem. Soc., Faraday Trans. 1* **1972**, *68*, 229-236. DOI: 10.1039/F19726800229.

(106) Schmickler, W.; Trasatti, S. Comment on “Trends in the Exchange Current for Hydrogen Evolution” [*J. Electrochem. Soc.*, *152*, J23 (2005)]. *Journal of The Electrochemical Society* **2006**, *153* (12), L31. DOI: 10.1149/1.2358294.

(107) Quaino, P.; Juarez, F.; Santos, E.; Schmickler, W. Volcano plots in hydrogen electrocatalysis – uses and abuses. *Beilstein Journal of Nanotechnology* **2014**, *5*, 846 - 854. DOI: 10.3762/bjnano.5.96.

(108) Madon, R. J.; Iglesia, E. Catalytic reaction rates in thermodynamically non-ideal systems. *J. Mol. Catal. A: Chem.* **2000**, *163* (1), 189-204. DOI: 10.1016/S1381-1169(00)00386-1.

(109) Schwartz, T. J.; Bond, J. Q. Leveraging De Donder relations for a thermodynamically rigorous analysis of reaction kinetics in liquid media. *J. Catal.* **2021**, *404*, 687-705. DOI: 10.1016/j.jcat.2021.09.026.

(110) Bates, J. S.; Gounder, R. Kinetic effects of molecular clustering and solvation by extended networks in zeolite acid catalysis. *Chem. Sci.* **2021**, *12* (13), 4699-4708. DOI: 10.1039/D1SC00151E.

(111) This section and the quotes below were adapted from Gileadi, E. In *Electrode Kinetics for Chemists, Chemical Engineers, and Materials Scientists*, Wiley VCH, 1996; pp 261-271.

(112) Nørskov, J. K.; Bligaard, T.; Hvolbæk, B.; Abild-Pedersen, F.; Chorkendorff, I.; Christensen, C. H. The nature of the active site in heterogeneous metal catalysis. *Chem. Soc. Rev.* **2008**, *37* (10), 2163-2171, 10.1039/B800260F. DOI: 10.1039/B800260F.

(113) Greeley, J. Theoretical Heterogeneous Catalysis: Scaling Relationships and Computational Catalyst Design. *Annual Review of Chemical and Biomolecular Engineering* **2016**, *7* (Volume 7, 2016), 605-635. DOI: 10.1146/annurev-chembioeng-080615-034413.

(114) Boudart, M. Two-step catalytic reactions. *AlChE J.* **1972**, *18* (3), 465-478. DOI: 10.1002/aic.690180303.

(115) Motagamwala, A. H.; Dumesic, J. A. Chemical kinetics for generalized two-step reaction schemes. *J. Catal.* **2021**, *404*, 850-863. DOI: 10.1016/j.jcat.2021.08.046.

(116) Clarke, T. B.; Krushinski, L. E.; Vannoy, K. J.; Colón-Quintana, G.; Roy, K.; Rana, A.; Renault, C.; Hill, M. L.; Dick, J. E. Single Entity Electrocatalysis. *Chem. Rev.* **2024**. DOI: 10.1021/acs.chemrev.3c00723.

(117) Mayer, J. M. Bonds over Electrons: Proton Coupled Electron Transfer at Solid–Solution Interfaces. *Journal of the American Chemical Society* **2023**, *145* (13), 7050-7064. DOI: 10.1021/jacs.2c10212.

(118) Agarwal, R. G.; Coste, S. C.; Groff, B. D.; Heuer, A. M.; Noh, H.; Parada, G. A.; Wise, C. F.; Nichols, E. M.; Warren, J. J.; Mayer, J. M. Free Energies of Proton-Coupled Electron Transfer Reagents and Their Applications. *Chem. Rev.* **2022**, *122* (1), 1-49. DOI: 10.1021/acs.chemrev.1c00521.

(119) Savara, A. Standard States for Adsorption on Solid Surfaces: 2D Gases, Surface Liquids, and Langmuir

Adsorbates. *The Journal of Physical Chemistry C* **2013**, *117* (30), 15710-15715. DOI: 10.1021/jp404398z.

(120) Campbell, C. T.; Sprowl, L. H.; Árnadóttir, L. Equilibrium Constants and Rate Constants for Adsorbates: Two-Dimensional (2D) Ideal Gas, 2D Ideal Lattice Gas, and Ideal Hindered Translator Models. *The Journal of Physical Chemistry C* **2016**, *120* (19), 10283-10297. DOI: 10.1021/acs.jpcc.6b00975.

(121) Savara, A. Comment on "Equilibrium Constants and Rate Constants for Adsorbates: Two-Dimensional (2D) Ideal Gas, 2D Ideal Lattice Gas, and Ideal Hindered Translator Models". *The Journal of Physical Chemistry C* **2016**, *120* (36), 20478-20480. DOI: 10.1021/acs.jpcc.6b07553.

(122) Savara, A. Correction to "Comment on 'Equilibrium Constants and Rate Constants for Adsorbates: 2D Ideal Gas, 2D Ideal Lattice Gas, and Ideal Hindered Translator Models'". *The Journal of Physical Chemistry C* **2017**, *121* (27), 14990-14992. DOI: 10.1021/acs.jpcc.7b05171.

(123) Campbell, C. T.; Sprowl, L. H.; Árnadóttir, L. Reply to "Comment on 'Equilibrium Constants and Rate Constants for Adsorbates: Two-Dimensional (2D) Ideal Gas, 2D Ideal Lattice Gas, and Ideal Hindered Translator Models'". *The Journal of Physical Chemistry C* **2016**, *120* (36), 20481-20482. DOI: 10.1021/acs.jpcc.6b07756.

(124) Chu, K. H.; Tan, B. C. Is the Frumkin (Fowler–Guggenheim) adsorption isotherm a two- or three-parameter equation? *Colloid and Interface Science Communications* **2021**, *45*, 100519. DOI: 10.1016/j.colcom.2021.100519.

(125) Campbell, C. T. Energies of Adsorbed Catalytic Intermediates on Transition Metal Surfaces: Calorimetric Measurements and Benchmarks for Theory. *Acc. Chem. Res.* **2019**, *52* (4), 984-993. DOI: 10.1021/acs.accounts.8b00579.

(126) Silbaugh, T. L.; Campbell, C. T. Energies of Formation Reactions Measured for Adsorbates on Late Transition Metal Surfaces. *The Journal of Physical Chemistry C* **2016**, *120* (44), 25161-25172. DOI: 10.1021/acs.jpcc.6b06154.

(127) Christmann, K. Interaction of hydrogen with solid surfaces. *Surf. Sci. Rep.* **1988**, *9* (1), 1-163. DOI: 10.1016/0167-5729(88)90009-X.

(128) Christmann, K. R. Hydrogen Sorption on Pure Metal Surfaces. In *Hydrogen Effects in Catalysis: Fundamentals and Practical Applications*, Paal, Z., Menon, P. G. Eds.; CRC Press, 1987; pp 1-53.

(129) Dong, Y.; Hu, G.; Hu, X.; Xie, G.; Lu, J.; Luo, M. Hydrogen Adsorption and Oxidation on Pt Film: An in Situ Real-Time Attenuated Total Reflection Infrared (ATR-IR) Spectroscopic Study. *The Journal of Physical Chemistry C* **2013**, *117* (24), 12537-12543. DOI: 10.1021/jp401427j.

(130) Conway, B. E.; Tilak, B. V. Interfacial processes involving electrocatalytic evolution and oxidation of H_2, and the role of chemisorbed H. *Electrochim. Acta* **2002**, *47* (22), 3571-3594. DOI: 10.1016/S0013-4686(02)00329-8.

(131) Conway, B. E.; Bai, L. Determination of the adsorption behaviour of 'overpotential-deposited' hydrogen-atom species in the cathodic hydrogen-evolution reaction by analysis of potential-relaxation transients. *J. Chem. Soc., Faraday Trans. 1* **1985**, *81* (8), 1841-1862. DOI: 10.1039/F19858101841.

(132) Pery, T.; Pelzer, K.; Buntkowsky, G.; Philippot, K.; Limbach, H.-H.; Chaudret, B. Direct NMR Evidence for the Presence of Mobile Surface Hydrides on Ruthenium Nanoparticles. *ChemPhysChem* **2005**, *6* (4), 605-607. DOI: 10.1002/cphc.200400621.

(133) Zheng, J.; Sheng, W.; Zhuang, Z.; Xu, B.; Yan, Y. Universal dependence of hydrogen oxidation and evolution reaction activity of platinum-group metals on pH and hydrogen binding energy. *Sci. Adv.* **2016**, *2* (3), e1501602. DOI: 10.1126/sciadv.1501602.

(134) Sherbo, R. S.; Moreno-Gonzalez, M.; Johnson, N. J. J.; Dvorak, D. J.; Fork, D. K.; Berlinguette, C. P. Accurate Coulometric Quantification of Hydrogen Absorption in Palladium Nanoparticles and Thin Films. *Chemistry of Materials* **2018**, *30* (12), 3963-3970. DOI: 10.1021/acs.chemmater.8b01324.

(135) Botello, L. E.; Feliu, J. M.; Climent, V. Activation Energy of Hydrogen Adsorption on Pt(111) in Alkaline Media: An Impedance Spectroscopy Study at Variable Temperatures. *ACS Appl. Mater. Interfaces* **2020**, *12* (38), 42911-42917. DOI: 10.1021/acsami.0c13158.

(136) Bai, Y.; Chen, B. W. J.; Peng, G.; Mavrikakis, M. Density functional theory study of thermodynamic and kinetic isotope effects of H_2/D_2 dissociative adsorption on transition metals. *Catalysis Science & Technology* **2018**, *8* (13), 3321-3335, DOI: 10.1039/C8CY00878G.

(137) Lam, Y.-C.; Soudackov, A. V.; Hammes-Schiffer, S. Theory of Electrochemical Proton-Coupled Electron Transfer in Diabatic Vibronic Representation: Application to Proton Discharge on Metal Electrodes in Alkaline Solution. *The Journal of Physical Chemistry C* **2020**, *124* (50), 27309-27322. DOI: 10.1021/acs.jpcc.0c08096.

(138) Wang, H.-X.; Toh, W. L.; Tang, B. Y.; Surendranath, Y. Metal surfaces catalyse polarization-dependent hydride transfer from H_2. *Nat. Catal.* **2023**, 6, 351–362 DOI: 10.1038/s41929-023-00944-1.

(139) García, G.; Koper, M. T. M. Stripping voltammetry of carbon monoxide oxidation on stepped platinum single-crystal electrodes in alkaline solution. *Physical Chemistry Chemical Physics* **2008**, *10* (25), 3802-3811. DOI: 10.1039/B803503M.

(140) Yang, Y.; Agarwal, R. G.; Hutchison, P.; Rizo, R.; Soudackov, A. V.; Lu, X.; Herrero, E.; Feliu, J. M.; Hammes-Schiffer, S.; Mayer, J. M.; Abruña, H. D. Inverse kinetic isotope effects in the oxygen reduction reaction at platinum single crystals. *Nat. Chem.* **2023**, *15* (2), 271-277. DOI: 10.1038/s41557-022-01084-y.

(141) McCrum, I. T.; Koper, M. T. M. The role of adsorbed hydroxide in hydrogen evolution reaction kinetics on modified platinum. *Nat. Energy* **2020**, *5* (11), 891-899. DOI: 10.1038/s41560-020-00710-8.

(142) Intikhab, S.; Snyder, J. D.; Tang, M. H. Adsorbed Hydroxide Does Not Participate in the Volmer Step of Alkaline Hydrogen Electrocatalysis. *ACS Catalysis* **2017**, *7* (12), 8314-8319. DOI: 10.1021/acscatal.7b02787.

(143) Markovic, N. M.; Grgur, B. N.; Ross, P. N. Temperature-Dependent Hydrogen Electrochemistry on Platinum Low-Index Single-Crystal Surfaces in Acid Solutions. *The journal of physical chemistry B* **1997**, *101* (27), 5405 - 5413. DOI: 10.1021/jp970930d.

(144) Conway, B. E.; Bai, L. Determination of adsorption of OPD H species in the cathodic hydrogen evolution reaction at Pt in relation to electrocatalysis. *J. Electroanal. Chem. Interfacial Electrochem.* **1986**, *198* (1), 149-175. DOI: 10.1016/0022-0728(86)90033-1.

(145) Conway, B. E.; Bai, L. State of adsorption and coverage by overpotential-deposited H in the H_2 evolution reaction at Au and Pt. *Electrochim. Acta* **1986**, *31* (8), 1013-1024. DOI: 10.1016/0013-4686(86)80017-2.

(146) Fujita, M.; Yamamoto, A.; Tsuchiya, N.; Yoshida, H. Hydrogen Adsorption/Desorption Isotherms on Supported

Platinum Nanoparticles Determined by in-situ XAS and ΔXANES Analysis. *ChemCatChem* **2022**, *14* (5), e202101709. DOI: 10.1002/cctc.202101709.

(147) Zhu, S.; Qin, X.; Yao, Y.; Shao, M. pH-Dependent Hydrogen and Water Binding Energies on Platinum Surfaces as Directly Probed through Surface-Enhanced Infrared Absorption Spectroscopy. *Journal of the American Chemical Society* **2020**, *142* (19), 8748-8754. DOI: 10.1021/jacs.0c01104.

(148) Tang, M. T.; Liu, X.; Ji, Y.; Norskov, J. K.; Chan, K. Modeling Hydrogen Evolution Reaction Kinetics through Explicit Water–Metal Interfaces. *The Journal of Physical Chemistry C* **2020**, *124* (51), 28083-28092. DOI: 10.1021/acs.jpcc.0c08310.

(149) Song, F.; Bai, L.; Moysiadou, A.; Lee, S.; Hu, C.; Liardet, L.; Hu, X. Transition Metal Oxides as Electrocatalysts for the Oxygen Evolution Reaction in Alkaline Solutions: An Application-Inspired Renaissance. *Journal of the American Chemical Society* **2018**, *140* (25), 7748-7759. DOI: 10.1021/jacs.8b04546.

(150) Yu, M.; Budiyanto, E.; Tüysüz, H. Principles of Water Electrolysis and Recent Progress in Cobalt-, Nickel-, and Iron-Based Oxides for the Oxygen Evolution Reaction. *Angewandte Chemie International Edition* **2022**, *61* (1), e202103824. DOI: 0.1002/anie.202103824.

(151) Kim, J. S.; Kim, B.; Kim, H.; Kang, K. Recent Progress on Multimetal Oxide Catalysts for the Oxygen Evolution Reaction. *Advanced Energy Materials* **2018**, *8* (11), 1702774. DOI: 10.1002/aenm.201702774.

(152) Chen, B. H.-Y.; Chang, H.-L. R. Development of low temperature three-way catalysts for future fuel efficient vehicles. *Johnson Matthey Technology Review* **2015**, *59* (1), 64-67.

(153) Gorte, R. J. Ceria in catalysis: From automotive applications to the water–gas shift reaction. *AlChE J.* **2010**, *56* (5), 1126-1135. DOI: 10.1002/aic.12234.

(154) Campbell, C. T.; Sauer, J. Introduction: Surface Chemistry of Oxides. *Chem. Rev.* **2013**, *113* (6), 3859-3862. DOI: 10.1021/cr4002337.

(155) Campbell, C. T.; Sellers, J. R. V. Enthalpies and Entropies of Adsorption on Well-Defined Oxide Surfaces: Experimental Measurements. *Chem. Rev.* **2013**, *113* (6), 4106-4135. DOI: 10.1021/cr300329s.

(156) Stumm, W.; Morgan, J. J. Aquatic Chemistry: Chemical Equilibria and Rates in Natural Waters, Chapters 7, 9, and 13, pp 349-424, 516-613, and 760-817; Wiley-Interscience, 1995.

(157) Pourbaix, M. *Atlas of Electrochemical Equilibria in Aqueous Solutions*; National Association of Corrosion Engineers, 1974.

(158) Burgess, D. R. J. Thermochemical Data. In *NIST Chemistry WebBook, NIST Standard Reference Database Number 69*, Linstrom, P. J., Mallard, W. G. Eds.; National Institute of Standards and Technology, (retrieved December 18, 2023).

(159) Van de Walle, C. G.; Neugebauer, J. Hydrogen in Semiconductors. *Annu. Rev. Mater. Res.* **2006**, *36* (1), 179-198. DOI: 10.1146/annurev.matsci.36.010705.155428.

(160) Al-Abadleh, H. A.; Grassian, V. H. Oxide surfaces as environmental interfaces. *Surf. Sci. Rep.* **2003**, *52* (3), 63-161. DOI: 10.1016/j.surfrep.2003.09.001.

(161) Damatov, D.; Laga, S. M.; Mader, E. A.; Peng, J.; Agarwal, R. G.; Mayer, J. M. Redox Reactivity of Colloidal Nanoceria and Use of Optical Spectra as an *In Situ* Monitor of Ce Oxidation States. *Inorganic Chemistry* **2018**, *57* (22), 14401-14408. DOI: 10.1021/acs.inorgchem.8b02598.

(162) Agarwal, R. G.; Kim, H.-J.; Mayer, J. M. Nanoparticle O–H Bond Dissociation Free Energies from Equilibrium Measurements of Cerium Oxide Colloids. *Journal of the American Chemical Society* **2021**, *143* (7), 2896-2907. DOI: 10.1021/jacs.0c12799.

(163) Agarwal, R. G.; Mayer, J. M. Coverage-Dependent Rate-Driving Force Relationships: Hydrogen Transfer from Cerium Oxide Nanoparticle Colloids. *Journal of the American Chemical Society* **2022**, *144* (45), 20699-20709. DOI: 10.1021/jacs.2c07988.

(164) Wise, C. F.; Mayer, J. M. Electrochemically Determined O–H Bond Dissociation Free Energies of NiO Electrodes Predict Proton-Coupled Electron Transfer Reactivity. *J. Am. Chem. Soc.* **2019**, *141* (38), 14971-14975. DOI: 10.1021/jacs.9b07923.

(165) Noh, H.; Mayer, J. M. Medium-independent hydrogen atom binding isotherms of nickel oxide electrodes. *Chem* **2022**, *8*, 3324-3345. DOI: 10.1016/j.chempr.2022.08.018.

(166) Naito, T.; Shinagawa, T.; Nishimoto, T.; Takanabe, K. Recent advances in understanding oxygen evolution reaction mechanisms over iridium oxide. *Inorganic Chemistry Frontiers* **2021**, *8* (11), 2900-2917. DOI: 10.1039/D0QI01465F.

(167) She, L.; Zhao, G.; Ma, T.; Chen, J.; Sun, W.; Pan, H. On the Durability of Iridium-Based Electrocatalysts toward the Oxygen Evolution Reaction under Acid Environment. *Adv. Funct. Mater.* **2022**, *32* (5), 2108465. DOI: 10.1002/adfm.202108465.

(168) Rao, R. R.; Kolb, M. J.; Halck, N. B.; Pedersen, A. F.; Mehta, A.; You, H.; Stoerzinger, K. A.; Feng, Z.; Hansen, H. A.; Zhou, H.; et al. Towards identifying the active sites on RuO_2(110) in catalyzing oxygen evolution. *Energy & Environmental Science* **2017**, *10* (12), 2626-2637. DOI: 10.1039/C7EE02307C.

(169) Liang, C.; Katayama, Y.; Tao, Y.; Morinaga, A.; Moss, B.; Celorrio, V.; Ryan, M.; Stephens, I. E.; Durrant, J. R.; Rao, R. R. Role of electrolyte pH on water oxidation for iridium oxides. *Journal of the American Chemical Society* **2024**, *146* (13), 8928–8938. DOI: 10.1021/jacs.3c12011.

(170) Zhou, Z.; Kan, E.; Deng, K.; Ogitsu, T.; Pham, T. A.; Zhan, C. Synergic Effects of Surface Chemistry and Applied Potentials on the Kinetics of the Electrocatalytic Oxygen Evolution Reaction in IrO_2. *ACS Applied Energy Materials* **2023**, *6* (23), 11963-11972. DOI: 10.1021/acsaem.3c02136.

(171) Kuo, D.-Y.; Kawasaki, J. K.; Nelson, J. N.; Kloppenburg, J.; Hautier, G.; Shen, K. M.; Schlom, D. G.; Suntivich, J. Influence of Surface Adsorption on the Oxygen Evolution Reaction on IrO_2(110). *Journal of the American Chemical Society* **2017**, *139* (9), 3473-3479. DOI: 10.1021/jacs.6b11932.

(172) Hu, B.; Kuo, D.-Y.; Paik, H.; Schlom, D. G.; Suntivich, J. Enthalpy and entropy of oxygen electroadsorption on RuO_2(110) in alkaline media. *The Journal of Chemical Physics* **2020**, *152* (9), 094704. DOI: 10.1063/1.5139049.

(173) Liang, C.; Katayama, Y.; Tao, Y.; Morinaga, A.; Moss, B.; Celorrio, V.; Ryan, M.; Stephens, I. E. L.; Durrant, J. R.; Rao, R. R. Role of Electrolyte pH on Water Oxidation for Iridium Oxides. *Journal of the American Chemical Society* **2024**, *146* (13), 8928-8938. DOI: 10.1021/jacs.3c12011.

(174) Lyons, M. E. G.; Floquet, S. Mechanism of oxygen reactions at porous oxide electrodes . Part 2—Oxygen evolution at RuO_2 , IrO_2 and $Ir_xRu_{1-x}O_2$ electrodes in aqueous acid and alkaline solution. *Physical Chemistry Chemical Physics* **2011**, *13* (12), 5314-5335. DOI: 10.1039/c0cp02875d PMID - 21344102.

(175) Nong, H. N.; Falling, L. J.; Bergmann, A.; Klingenhof, M.; Tran, H. P.; Spöri, C.; Mom, R.; Timoshenko, J.; Zichittella, G.; Knop-Gericke, A.; et al. Key role of chemistry versus bias in electrocatalytic oxygen evolution. *Nature* **2020**, *587* (7834), 408-413. DOI: 10.1038/s41586-020-2908-2.

(176) JenningsAnodes. *Chlor Alkali*. https://jenningsanodes.com/applications/chlor-alkali/ (accessed accessed 27July2024.

(177) Choi, S.; Choi, W. I.; Lee, J.-S.; Lee, C. H.; Balamurugan, M.; Schwarz, A. D.; Choi, Z. S.; Randriamahazaka, H.; Nam, K. T. A Reflection on Sustainable Anode Materials for Electrochemical Chloride Oxidation. *Adv. Mater.* **2023**, *35* (43), 2300429. DOI: 10.1002/adma.202300429.

(178) Goryachev, A.; Etzi Coller Pascuzzi, M.; Carlà, F.; Weber, T.; Over, H.; Hensen, E. J. M.; Hofmann, J. P. Electrochemical stability of RuO_2(110)/Ru(0001) model electrodes in the oxygen and chlorine evolution reactions. *Electrochim. Acta* **2020**, *336*, 135713. DOI: 10.1016/j.electacta.2020.135713.

(179) Narangoda, P.; Spanos, I.; Masa, J.; Schlögl, R.; Zeradjanin, A. R. Electrocatalysis Beyond 2020: How to Tune the Preexponential Frequency Factor. *ChemElectroChem* **2022**, *9* (4), e202101278. DOI: 10.1002/celc.202101278.

(180) Velasco-Vélez, J.-J.; Carbonio, E. A.; Chuang, C.-H.; Hsu, C.-J.; Lee, J.-F.; Arrigo, R.; Hävecker, M.; Wang, R.; Plodinec, M.; Wang, F. R.; et al. Surface Electron-Hole Rich Species Active in the Electrocatalytic Water Oxidation. *Journal of the American Chemical Society* **2021**, *143* (32), 12524-12534. DOI: 10.1021/jacs.1c01655.

(181) Geppert, J.; Kubannek, F.; Röse, P.; Krewer, U. Identifying the oxygen evolution mechanism by microkinetic modelling of cyclic voltammograms. *Electrochim. Acta* **2021**, *380*, 137902. DOI: 10.1016/j.electacta.2021.137902.

(182) Czioska, S.; Boubnov, A.; Escalera-López, D.; Geppert, J.; Zagalskaya, A.; Röse, P.; Saraçi, E.; Alexandrov, V.; Krewer, U.; Cherevko, S.; et al. Increased Ir–Ir Interaction in Iridium Oxide during the Oxygen Evolution Reaction at High Potentials Probed by Operando Spectroscopy. *ACS Catalysis* **2021**, *11* (15), 10043-10057. DOI: 10.1021/acscatal.1c02074.

(183) Fleischmann, S.; Mitchell, J. B.; Wang, R.; Zhan, C.; Jiang, D.-e.; Presser, V.; Augustyn, V. Pseudocapacitance: From Fundamental Understanding to High Power Energy Storage Materials. *Chem. Rev.* **2020**, *120* (14), 6738-6782. DOI: 10.1021/acs.chemrev.0c00170.

(184) Stoerzinger, K. A.; Rao, R. R.; Wang, X. R.; Hong, W. T.; Rouleau, C. M.; Shao-Horn, Y. The Role of Ru Redox in pH-Dependent Oxygen Evolution on Rutile Ruthenium Dioxide Surfaces. *Chem* **2017**, *2* (5), 668-675. DOI: 10.1016/j.chempr.2017.04.001.

(185) Gentry, N. E.; Gibson, N. J.; Lee, J. L.; Mayer, J. M. Trap States in Reduced Colloidal Titanium Dioxide Nanoparticles Have Different Proton Stoichiometries. **2024**, submitted.

(186) Pang, C. L.; Lindsay, R.; Thornton, G. Structure of Clean and Adsorbate-Covered Single-Crystal Rutile TiO_2 Surfaces. *Chem. Rev.* **2013**, *113* (6), 3887-3948. DOI: 10.1021/cr300409r.

(187) Henderson, M. A.; Lyubinetsky, I. Molecular-Level Insights into Photocatalysis from Scanning Probe Microscopy Studies on TiO_2(110). *Chem. Rev.* **2013**, *113* (6), 4428-4455. DOI: 10.1021/cr300315m.

(188) Finklea, H. O. Chapter 2: Titanium Dioxide (TiO_2) and Strontium Titanate ($SrTiO_3$). In *Semiconductor electrodes*, Finklea, H. O. Ed.; Elsevier, 1988; pp 42–154.

(189) Chen, X.; Selloni, A. Introduction: Titanium Dioxide (TiO_2) Nanomaterials. *Chem. Rev.* **2014**, *114* (19), 9281-9282. DOI: 10.1021/cr500422r.

(190) Warburton, R. E.; Mayer, J. M.; Hammes-Schiffer, S. Proton-Coupled Defects Impact O–H Bond Dissociation Free Energies on Metal Oxide Surfaces. *The Journal of Physical Chemistry Letters* **2021**, *12* (40), 9761-9767. DOI: 10.1021/acs.jpclett.1c02837.

(191) Peper, J. L.; Gentry, N. E.; Boudy, B.; Mayer, J. M. Aqueous TiO_2 Nanoparticles React by Proton-Coupled Electron Transfer. *Inorganic Chemistry* **2022**, *61* (2), 767-777. DOI: 10.1021/acs.inorgchem.1c03125.

(192) Darcy, J. W.; Koronkiewicz, B.; Parada, G. A.; Mayer, J. M. A Continuum of Proton-Coupled Electron Transfer Reactivity. *Acc Chem Res* **2018**, *51* (10), 2391-2399. DOI: 10.1021/acs.accounts.8b00319.

(193) Corma, A.; Llopis, F.; Monton, J. B.; Weller, S. W. Comparison of models in heterogeneous catalysis for ideal and non-ideal surfaces. *Chem. Eng. Sci.* **1988**, *43* (4), 785-792. DOI: 10.1016/0009-2509(88)80073-3.

(194) Bandstra, J. Z.; Tratnyek, P. G. Applicability of Single-Site Rate Equations for Reactions on Inhomogeneous Surfaces. *Industrial & Engineering Chemistry Research* **2004**, *43* (7), 1615-1622. DOI: 10.1021/ie034250a.

(195) Murzin, D. Y. On Surface Heterogeneity and Catalytic Kinetics. *Industrial & Engineering Chemistry Research* **2005**, *44* (6), 1688-1697. DOI: 10.1021/ie049044x.

(196) Broadbelt, L. J.; Rekoske, J. E. Necessary levels of detail in microkinetic models of catalytic reactions on nonuniform surfaces. *Chem. Eng. Sci.* **1996**, *51* (12), 3337-3347. DOI: 10.1016/0009-2509(95)00385-1.

(197) Reference 92[Universal…Nørskov] indirectly addresses the issue of similarity in its Section VI.i and the possible variation in alpha in Section VI.iii: “the accuracy of the linear BEP relations will depend strongly on the adsorbate and the range of metals studied. For the metals considered herein, the mixing of the transition state with the surface is very similar to that of the final state and hence the transition state energies taken relative to relevant gas phase species will scale with the final state energies.”.

(198) Wyvratt, B. M.; Gaudet, J. R.; Pardue, D. B.; Marton, A.; Rudić, S.; Mader, E. A.; Cundari, T. R.; Mayer, J. M.; Thompson, L. T. Reactivity of Hydrogen on and in Nanostructured Molybdenum Nitride: Crotonaldehyde Hydrogenation. *ACS Catalysis* **2016**, *6* (9), 5797-5806. DOI: 10.1021/acscatal.6b00936.

(199) Gennero de Chialvo, M. R.; Chialvo, A. C. Kinetics of hydrogen evolution reaction with Frumkin adsorption: re-examination of the Volmer–Heyrovsky and Volmer–Tafel routes. *Electrochim. Acta* **1998**, *44* (5), 841-851. DOI: 10.1016/S0013-4686(98)00233-3.

(200) Shen, D.; Liu, Y.; Yang, G.; Yu, H.; Peng, F. Mechanistic Insights into Cyclic Voltammograms on Pt(111): Kinetics Simulations. *ChemPhysChem* **2019**, *20* (21), 2791-2798. DOI: 10.1002/cphc.201900804.

(201) Dion, F.; Lasia, A. The use of regularization methods in the deconvolution of underlying distributions in electrochemical processes. *Journal of Electroanalytical Chemistry* **1999**, *475* (1), 28-37. DOI: 10.1016/S0022-0728(99)00334-4.

(202) Biegler, T.; Woods, R. Effects of neglecting pre-exponential terms in electrochemical kinetic equations. *J. Electroanal. Chem. Interfacial Electrochem.* **1969**, *20* (3), 347-356. DOI: 10.1016/S0022-0728(69)80163-4.

(203) Guidelli, R.; Compton, R. G.; Feliu, J. M.; Gileadi, E.; Lipkowski, J.; Schmickler, W.; Trasatti, S. Defining the

transfer coefficient in electrochemistry: An assessment (IUPAC Technical Report). **2014**, *86* (2), 245-258. DOI: 10.1515/pac-2014-5026.

(204) Grant, P. G.; Lemke, S. L.; Dwyer, M. R.; Phillips, T. D. Modified Langmuir Equation for S-Shaped and Multisite Isotherm Plots. *Langmuir* **1998**, *14* (15), 4292-4299. DOI: 10.1021/la971218a.

(205) Quaino, P. M.; Gennero de Chialvo, M. R.; Chialvo, A. C. Hydrogen electrode reaction: A complete kinetic description. *Electrochim. Acta* **2007**, *52* (25), 7396-7403. DOI: 10.1016/j.electacta.2007.06.030.

(206) Conway, B. E.; Wilkinson, D. P. Brønsted relationships for heterogeneous proton transfer at electrode interfaces. *J. Chem. Soc., Faraday Trans. 1* **1988**, *84* (10), 3389-3400. DOI: 10.1039/F19888403389.

(207) Jackson, M. N.; Surendranath, Y. Donor-Dependent Kinetics of Interfacial Proton-Coupled Electron Transfer. *J Am Chem Soc* **2016**, *138* (9), 3228-3234. DOI: 10.1021/jacs.6b00167.

(208) Lewis, N. B.; Bisbey, R. P.; Westendorff, K. S.; Soudackov, A. V.; Surendranath, Y. A molecular-level mechanistic framework for interfacial proton-coupled electron transfer kinetics. *Nat. Chem.* **2024**, *16* (3), 343-352. DOI: 10.1038/s41557-023-01400-0.

(209) Tyburski, R.; Liu, T.; Glover, S. D.; Hammarström, L. Proton-Coupled Electron Transfer Guidelines, Fair and Square. *J Am Chem Soc* **2021**, *143* (2), 560-576. DOI: 10.1021/jacs.0c09106.

(210) Salamone, M.; Galeotti, M.; Romero-Montalvo, E.; van Santen, J. A.; Groff, B. D.; Mayer, J. M.; DiLabio, G. A.; Bietti, M. Bimodal Evans–Polanyi Relationships in Hydrogen Atom Transfer from C(sp^3)–H Bonds to the Cumyloxyl Radical. A Combined Time-Resolved Kinetic and Computational Study. *Journal of the American Chemical Society* **2021**, *143* (30), 11759-11776. DOI: 10.1021/jacs.1c05566.

(211) Qiu, G.; Knowles, R. R. Rate-Driving Force Relationships in the Multisite Proton-Coupled Electron Transfer Activation of Ketones. *J Am Chem Soc* **2019**, *141* (6), 2721-2730. DOI: 10.1021/jacs.8b13451.

(212) Schneider, J. E.; Goetz, M. K.; Anderson, J. S. Statistical analysis of C–H activation by oxo complexes supports diverse thermodynamic control over reactivity. *Chem. Sci.* **2021**, *12* (11), 4173-4183. DOI: 10.1039/D0SC06058E.

(213) Coste, S. C.; Brezny, A. C.; Koronkiewicz, B.; Mayer, J. M. C–H oxidation in fluorenyl benzoates does not proceed through a stepwise pathway: revisiting asynchronous proton-coupled electron transfer. *Chem. Sci.* **2021**, *12* (39), 13127-13136. DOI: 10.1039/D1SC03344A.

(214) Gerischer, H. Mechanismus der Elektrolytischen Wasserstoffabscheidung und Adsorptionsenergie von Atomarem Wasserstoff. *Bull. Soc. Chim. Belg.* **1958**, *67* (7-8), 506-527. DOI: 10.1002/bscb.19580670714.

(215) Conway, B. E.; Bockris, J. O. M. Electrolytic Hydrogen Evolution Kinetics and Its Relation to the Electronic and Adsorptive Properties of the Metal. *The Journal of Chemical Physics* **1957**, *26* (3), 532-541. DOI: 10.1063/1.1743339.

(216) Rüetschi, P.; Delahay, P. Hydrogen Overvoltage and Electrode Material. A Theoretical Analysis. *The Journal of Chemical Physics* **1955**, *23* (1), 195-199. DOI: 10.1063/1.1740527.

(217) Trasatti, S. Work function, electronegativity, and electrochemical behaviour of metals: III. Electrolytic hydrogen evolution in acid solutions. *J. Electroanal. Chem. Interfacial Electrochem.* **1972**, *39* (1), 163-184. DOI: 10.1016/S0022-0728(72)80485-6.

(218) Nørskov, J. K.; Bligaard, T.; Logadottir, A.; Bahn, S.; Hansen, L. B.; Bollinger, M.; Bengaard, H.; Hammer, B.; Sljivancanin, Z.; Mavrikakis, M.; et al. Universality in Heterogeneous Catalysis. *J. Catal.* **2002**, *209* (2), 275-278. DOI: 10.1006/jcat.2002.3615.

(219) Man, I. C.; Su, H.-Y.; Calle-Vallejo, F.; Hansen, H. A.; Martínez, J. I.; Inoglu, N. G.; Kitchin, J.; Jaramillo, T. F.; Nørskov, J. K.; Rossmeisl, J. Universality in Oxygen Evolution Electrocatalysis on Oxide Surfaces. *ChemCatChem* **2011**, *3* (7), 1159-1165. DOI: 10.1002/cctc.201000397 (acccessed 2023/03/19).

(220) Wang, S.; Petzold, V.; Tripkovic, V.; Kleis, J.; Howalt, J. G.; Skúlason, E.; Fernández, E. M.; Hvolbæk, B.; Jones, G.; Toftelund, A.; et al. Universal transition state scaling relations for (de)hydrogenation over transition metals. *Physical Chemistry Chemical Physics* **2011**, *13* (46), 20760-20765, 10.1039/C1CP20547A. DOI: 10.1039/C1CP20547A.

(221) Zeradjanin, A. R.; Grote, J.-P.; Polymeros, G.; Mayrhofer, K. J. J. A Critical Review on Hydrogen Evolution Electrocatalysis: Re-exploring the Volcano-relationship. *Electroanalysis* **2016**, *28* (10), 2256-2269. DOI: 10.1002/elan.201600270.

(222) Yang, T. T.; Patil, R. B.; McKone, J. R.; Saidi, W. A. Revisiting trends in the exchange current for hydrogen evolution. *Catalysis Science & Technology* **2021**, *11* (20), 6832-6838, 10.1039/D1CY01170G. DOI: 10.1039/D1CY01170G.

(223) Abild-Pedersen, F.; Lytken, O.; Engbæk, J.; Nielsen, G.; Chorkendorff, I.; Nørskov, J. K. Methane activation on Ni(111): Effects of poisons and step defects. *Surf. Sci.* **2005**, *590* (2), 127-137. DOI: 10.1016/j.susc.2005.05.057.

(224) Tsai, C.; Li, H.; Park, S.; Park, J.; Han, H. S.; Nørskov, J. K.; Zheng, X.; Abild-Pedersen, F. Electrochemical generation of sulfur vacancies in the basal plane of MoS_2 for hydrogen evolution. *Nature Communications* **2017**, *8* (1), 15113. DOI: 10.1038/ncomms15113.

(225) Weng, C.-C.; Ren, J.-T.; Yuan, Z.-Y. Transition Metal Phosphide-Based Materials for Efficient Electrochemical Hydrogen Evolution: A Critical Review. *ChemSusChem* **2020**, *13* (13), 3357-3375. DOI: 10.1002/cssc.202000416.

(226) Ge, Z.; Fu, B.; Zhao, J.; Li, X.; Ma, B.; Chen, Y. A review of the electrocatalysts on hydrogen evolution reaction with an emphasis on Fe, Co and Ni-based phosphides. *Journal of Materials Science* **2020**, *55* (29), 14081-14104. DOI: 10.1007/s10853-020-05010-w.

(227) Wu, Z.; Gan, Q.; Li, X.; Zhong, Y.; Wang, H. Elucidating Surface Restructuring-Induced Catalytic Reactivity of Cobalt Phosphide Nanoparticles under Electrochemical Conditions. *The Journal of Physical Chemistry C* **2018**, *122* (5), 2848-2853. DOI: 10.1021/acs.jpcc.7b11843.

(228) Delley, M. F.; Wu, Z.; Mundy, M. E.; Ung, D.; Cossairt, B. M.; Wang, H.; Mayer, J. M. Hydrogen on Cobalt Phosphide. *Journal of the American Chemical Society* **2019**, *141* (38), 15390-15402. DOI: 10.1021/jacs.9b07986.

(229) Hu, G.; Tang, Q.; Jiang, D.-e. CoP for hydrogen evolution: implications from hydrogen adsorption. *Physical Chemistry Chemical Physics* **2016**, *18* (34), 23864-23871. DOI: 10.1039/C6CP04011J.

(230) Kibsgaard, J.; Tsai, C.; Chan, K.; Benck, J. D.; Nørskov, J. K.; Abild-Pedersen, F.; Jaramillo, T. F. Designing an improved transition metal phosphide catalyst for hydrogen evolution using experimental and theoretical trends. *Energy & Environmental Science* **2015**, *8* (10), 3022-3029. Quote

is from the Supporting Information.
DOI: 10.1039/C5EE02179K.

(231) Musselwhite, N.; Somorjai, G. A. Investigations of Structure Sensitivity in Heterogeneous Catalysis: From Single Crystals to Monodisperse Nanoparticles. *Top. Catal.* **2013**, *56* (15), 1277-1283. DOI: 10.1007/s11244-013-0150-y.

(232) Goldsmith, Z. K.; Lam, Y. C.; Soudackov, A. V.; Hammes-Schiffer, S. Proton Discharge on a Gold Electrode from Triethylammonium in Acetonitrile: Theoretical Modeling of Potential-Dependent Kinetic Isotope Effects. *Journal of the American Chemical Society* **2019**, *141* (2), 1084-1090. DOI: 10.1021/jacs.8b11826.

(233) Costentin, C.; Porter, T. R.; Savéant, J. M. How Do Pseudocapacitors Store Energy? Theoretical Analysis and Experimental Illustration. *ACS Appl Mater Interfaces* **2017**, *9* (10), 8649-8658. DOI: 10.1021/acsami.6b14100.

(234) Costentin, C. Electrochemical Energy Storage: Questioning the Popular $v/v^{1/2}$ Scan Rate Diagnosis in Cyclic Voltammetry. *The Journal of Physical Chemistry Letters* **2020**, *11* (22), 9846-9849. DOI: 10.1021/acs.jpclett.0c02667.

(235) Gentry, N. E.; Kurimoto, A.; Cui, K.; Cleron, J. L.; Xiang, C. M.; Hammes-Schiffer, S.; Mayer, J. M. Hydrogen on Colloidal Gold Nanoparticles. *Journal of the American Chemical Society* **2024**, *146* (21), 14505-14520. DOI: 10.1021/jacs.4c00507.

(236) Dwarica, N. S. Studies of Colloidal Iron Carbide Nanoparticle Fischer-Tropsch Catalysts: Characterizing Adsorption Sites and Reactivity Towards Hydrogen Atom Transfers. Ph.D., Yale University, United States -- Connecticut, 2023. https://www.proquest.com/dissertations-theses/studies-colloidal-iron-carbide-nanoparticle/docview/2834864661/se-2.

(237) Valdez, C. N.; Schimpf, A. M.; Gamelin, D. R.; Mayer, J. M. Proton-Controlled Reduction of ZnO Nanocrystals: Effects of Molecular Reductants, Cations, and Thermodynamic Limitations. *Journal of the American Chemical Society* **2016**, *138* (4), 1377-1385. DOI: 10.1021/jacs.5b12182.

(238) Valdez, C. N.; Delley, M. F.; Mayer, J. M. Cation Effects on the Reduction of Colloidal ZnO Nanocrystals. *Journal of the American Chemical Society* **2018**, *140* (28), 8924-8933. DOI: 10.1021/jacs.8b05144.

(239) Saouma, C. T.; Tsou, C.-C.; Richard, S.; Ameloot, R.; Vermoortele, F.; Smolders, S.; Bueken, B.; DiPasquale, A. G.; Kaminsky, W.; Valdez, C. N.; De Vos, D. E.; Mayer, J. M. Sodium-coupled electron transfer reactivity of metal–organic frameworks containing titanium clusters: the importance of cations in redox chemistry. *Chem. Sci.* **2019**, *10* (5), 1322-1331, DOI: 10.1039/C8SC04138E.

(240) Samantaray, Y.; Martin, D. J.; Agarwal, R. G.; Gibson, N. J.; Mayer, J. M. Proton-Coupled Electron Transfer of Cerium Oxide Nanoparticle Thin-Film Electrodes. *The Journal of Physical Chemistry C* **2023**, *127* (8), 4015-4020. DOI: 10.1021/acs.jpcc.2c06783.

(241) Weckhuysen, B. M. Snapshots of a working catalyst: possibilities and limitations of in situ spectroscopy in the field of heterogeneous catalysis. *Chem. Commun.* **2002**, (2), 97-110. DOI: 10.1039/B107686H.

(242) Zaera, F. Study of the surface chemistry of methyl iodide coadsorbed with hydrogen on Pt(111). *Surf. Sci.* **1992**, *262* (3), 335-350. DOI: 10.1016/0039-6028(92)90130-X.

(243) Ohsawa, K.; Yoshida, M.; Doi, T. A Direct and Mild Formylation Method for Substituted Benzenes Utilizing Dichloromethyl Methyl Ether–Silver Trifluoromethanesulfonate. *The Journal of Organic Chemistry* **2013**, *78* (7), 3438-3444. DOI: 10.1021/jo400056k.

(244) Wang, H.; Abruña, H. D. Adsorbed Enolate as the Precursor for the C–C Bond Splitting during Ethanol Electrooxidation on Pt. *Journal of the American Chemical Society* **2023**, *145* (11), 6330–6338. DOI: 10.1021/jacs.2c13401.

(245) Bakshi, H. B.; Lucky, C.; Chen, H.-S.; Schreier, M. Electrocatalytic Scission of Unactivated $C(sp^3)$–$C(sp^3)$ Bonds through Real-Time Manipulation of Surface-Bound Intermediates. *Journal of the American Chemical Society* **2023**, *145* (25), 13742-13749. DOI: 10.1021/jacs.3c02108.

(246) Zaera, F. In-situ and operando spectroscopies for the characterization of catalysts and of mechanisms of catalytic reactions. *J. Catal.* **2021**, *404*, 900-910. DOI: 10.1016/j.jcat.2021.08.013.

(247) Hammel, B. F.; Hall, L. M. G.; Pellows, L. M.; Pearce, O. M.; Tongying, P.; Yazdi, S.; Dukovic, G. Relationships between Compositional Heterogeneity and Electronic Spectra of $(Ga_{1-x}Zn_x)(N_{1-x}O_x)$ Nanocrystals Revealed by Valence Electron Energy Loss Spectroscopy. *The Journal of Physical Chemistry C* **2023**, *127* (16), 7762-7771. DOI: 10.1021/acs.jpcc.3c00572.

(248) Dery, S.; Friedman, B.; Shema, H.; Gross, E. Mechanistic Insights Gained by High Spatial Resolution Reactivity Mapping of Homogeneous and Heterogeneous (Electro)Catalysts. *Chem. Rev.* **2023**, *123* (9), 6003-6038. DOI: 10.1021/acs.chemrev.2c00867.

(249) Chen, Y.-S.; Liu, P.-Y.; Niu, R.; Devaraj, A.; Yen, H.-W.; Marceau, R. K. W.; Cairney, J. M. Atom Probe Tomography for the Observation of Hydrogen in Materials: A Review. *Microsc. Microanal.* **2023**, *29* (1), 1-15. DOI: 10.1093/micmic/ozac005.

(250) Kaida, T.; Kamioka, K.; Ida, T.; Kuriyama, K.; Kushida, K.; Kinomura, A. Rutherford backscattering and nuclear reaction analyses of hydrogen ion-implanted ZnO bulk single crystals. *Nuclear Instruments and Methods in Physics Research Section B: Beam Interactions with Materials and Atoms* **2014**, *332*, 15-18. DOI: 10.1016/j.nimb.2014.02.020.

(251) Constable, F. H. The mechanism of catalytic decomposition. *Proceedings of the Royal Society of London. Series A* **1925**, *108* (746), 355-378. DOI: 10.1098/rspa.1925.0081.

(252) Jagiello, J. Stable Numerical Solution of the Adsorption Integral Equation Using Splines. *Langmuir* **1994**, *10* (8), 2778-2785. DOI: 10.1021/la00020a045.

(253) Horányi, G.; Rizmayer, E. M. Role of adsorption phenomena in the electrocatalytic reduction of nitric acid at a platinized platinum electrode. *J. Electroanal. Chem. Interfacial Electrochem.* **1982**, *140* (2), 347-366. DOI: 10.1016/0022-0728(82)85178-4.

(254) Gritti, F.; Guiochon, G. Comparison between heterogeneous multi-Langmuir and homogeneous electrostatically modified Langmuir models in accounting for the adsorption of small organic ions in reversed-phase liquid chromatography. *J. Chromatogr. A* **2010**, *1217* (35), 5584-5594. DOI: 10.1016/j.chroma.2010.06.046.

(255) Sillar, K.; Hofmann, A.; Sauer, J. *Ab Initio* Study of Hydrogen Adsorption in MOF-5. *Journal of the American Chemical Society* **2009**, *131* (11), 4143-4150. DOI: 10.1021/ja8099079.

(256) Equation 21 was adapted from the model used in reference 257. That model assessed “the plausibility of bifunctional activity gains … in two ways: 1) a gain relative to the sum of the activities of the two considered decoupled catalysts

and 2) a gain relative to the activity of two sites on the optimal monofunctional catalyst." Thus, that study did not consider cases where the preferred mechanism *requires* the presence of neigboring different sites with different properties. For H_2 loss by $Mo_2N(H)_x$, for instance (in the next sentence in the text), H_2 seems to be preferentially formed in a polar mechanism from $MoH^{\partial-} + NH^{\partial+}$, a path that cannot be accessed without the bifunctionality.

(257) Andersen, M.; Medford, A. J.; Nørskov, J. K.; Reuter, K. Analyzing the Case for Bifunctional Catalysis. *Angewandte Chemie International Edition* **2016**, *55* (17), 5210-5214. DOI: 10.1002/anie.201601049.

(258) Limaye, A. M.; Zeng, J. S.; Willard, A. P.; Manthiram, K. Bayesian data analysis reveals no preference for cardinal Tafel slopes in CO_2 reduction electrocatalysis. *Nature Communications* **2021**, *12* (1), 703. DOI: 10.1038/s41467-021-20924-y.